An analysis of West African dynamics using a linearized GCM

Nicholson[1], S. E., A. I. Barcilon [2] and M. Challa[3]

[1]Florida State University

Department of Meteorology

Tallahassee FL 32306

[2]Visiting Scientist, MMM, NCAR,

PO Box 3000

Boulder, CO 80307

[3]Florida State University

Geophysical Fluid Dynamics Institute

Tallahassee FL 32306

Submitted to the *Journal of the Atmospheric Sciences*

April 2006

Revised, April 2007

ABSTRACT

This study utilizes a linear, primitive equation spherical model to study the development and propagation of easterly wave disturbances over West Africa. Perturbations are started from an initial disturbance consisting of a barotropic vortex and the governing equations are integrated forward in time. The perturbations are introduced into basic states corresponding to the observed dynamical and thermodynamical characteristics of two wet years in the Sahel and two dry years.

The model simulations show consistent contrasts in wave activity between the wet and dry years. The waves are markedly stronger in the wet years and show a barotropic structure throughout the troposphere. The waves tend to extend throughout the troposphere to the level of the Tropical Easterly Jet (TEJ) in the wet years, but not in the dry years. The upper tropospheric shear, which is stronger in wet years, appears to be a key factor in wave development. This shear is dependent on the intensity of the TEJ, suggesting that the TEJ is an important factor in interannual variability in the Sahel. When the overall shear is weak, vertical development is suppressed.

Another contrast is that in the dry years the growth rates show a single maximum around 3,000 to 4,000 km, but in wet years there is a second around 6,000 to 7,000 km. This suggests that both synoptic scale and planetary scale waves are active in the rainy season of some wet years. Imposing considerations of potential vorticity, the generation of planetary scale waves implies a strong link between the surface and the TEJ in wet years. Such a link is absent in the dry years. This is likely a major factor in the interannual variability of rainfall in the Sahel.

1.0 Introduction

The West African Sahel is a semi-arid strip along the southern border of the Sahara. Its summer rainfall regime is characterized by a high degree of variability that is evident on both interannual and decadal time scales (Fig. 1). In the 1950s rainfall averaged about 600 mm per year in the core of this region, i.e., in latitudes 14 ^{o} N to 16 ^{o} N. In the 1980s rainfall averaged roughly 400 mm per year in this same area (Nicholson 2005). Grist et al. (2002) suggested that contrasts in easterly wave activity in the wet and dry years might be a factor in this variability. A wavelet analysis clearly showed that during wet years the waves were stronger and waves with longer periods played a significant role.

It has long been accepted that the instabilities promoting wave development and growth are linked to the horizontal and vertical shear of the African Easterly Jet (AEJ), a moderate jetstream with its core at 650 mb to 700 mb over West Africa (Burpee 1972, Rennick 1981, Newell and Kidson 1979, 1984). Grist et al. (2002) further hypothesized that the fluctuations in rainfall could be linked to changes in the instabilities of the AEJ, with the instabilities modulating wave activity in ways to either *enhance* or *suppress* rainfall. The basic states of a four-year wet period (1958-61) and a four-year dry period (1982-85) were simulated using a linear, adiabatic, quasi-geostrophic model centered at 15 ^{o} N.

The method of solution utilized by Grist et al. (2002) was adapted from Kwon (1989). However, the spirit of the investigation was quite different from other investigations, including Kwon's, because observed data were used to construct the basic states of the model. The simulation showed that waves with larger growth rates, longer wavelengths and greater phase speeds develop on the basic state of the wet years, consistent with the observational analysis. An

analysis of the basic states further showed that for West Africa as a whole baroclinic and barotropic instability were of similar magnitude in the dry years, but in the wet years barotropic instability increased significantly and was the dominant mechanism of instability.

A shortcoming of the aforementioned study is that it examined *composites* of individual years that were selected on the basis of annual rainfall. The years within a composite may have differed in terms of the dynamic factors producing the rainfall conditions. In particular, Nicholson and Grist (2001) noted that fluctuations in the amount of seasonal rainfall in the Sahel could be produced by either a change in the intensity of the tropical rainbelt or a latitudinal shift of this zone over West Africa. The latter would modify the length of time the rainbelt influences the Sahelian latitudes. The different causal factors are evident, at least in part, through the spatial pattern of rainfall anomalies in individual years, as described in section 2.1.

In this study, contrasting years corresponding to both changes in intensity of the tropical rainbelt and to shifts in its latitudinal location are examined. A linear model is used to simulate wave growth by following the release of a perturbation in a zonal flow constructed using data that describes dynamics in the West African region. Detailed basic state plots of zonal wind, potential temperature and stratification of the summer months of different years provide a rich backdrop in which to understand the perturbations' growth. The basic states of two wet years, 1950 and 1955, and two dry years, 1983 and 1984 are investigated. Each month of the Sahel rainy season (i.e., June to September) is simulated. The pair 1950/1984 represents latitudinal shifts of the rainbelt and the pair 1955/1983 represents changes in its intensity. Thus, although 1950 was anomalously wet in the Sahel and 1984 was anomalously dry, the overall intensity of convection over West Africa during the summer rainy season was the same in both years.

It is noteworthy that the years 1950 and 1955 were considerably wetter in the Sahel than the composited "wet" years used by the Grist et al. study, in which the availability of upper air

data influenced the choice of years. The years 1983 and 1984 were two of the driest on record in the region, so that the four years represent an extreme range of conditions.

This study utilizes a *linear, primitive equation spherical* model, described in section 3. The model's architecture resembles that of GCMs. Perturbations are started from an initial disturbance consisting of an initial barotropic vortex placed over the region representing the West African land mass, i.e., north of the equator. Then the governing equations are integrated forward in time, allowing the perturbation to growth while keeping the zonal mean constant. Preliminary simulations utilized a 20-level version of the model. These showed that the main dynamics could be preserved when as few as 4 levels were retained.

The model is sufficiently different from that used by Grist et al. (2002), which was a *linear quasi-geostrophic channel model* centered on 15 ^{o} N and solved using a normal mode approach. The quasi-geographic assumption was appropriate because most of the West African dynamical processes take place near 15 ^{o} to 18 ^{o} N. However, the current model provides several advantages that give increased insight into the dynamical processes. For one, it follows the dynamical evolution resulting from the presence of a perturbation in the zonal flow. Also, the development can be reproduced one mode at a time. Finally, unlike the two-level model of Grist et al., the multi-level structure of the current model makes it possible to determine the level in the atmosphere (e.g., at the surface, or near the AEJ or TEJ) at which the growing mode commences and to track the development vertically.

The broad goal of our work is to understand the relationships between African Easterly Waves and the interannual variability of rainfall. In this study, the question can only be addressed indirectly by contrasting anomalously wet years/months with anomalously dry ones. Our approach is to ask the following question: if a perturbation ("disturbance") is introduced into

contrasting basic states, how will the resultant evolution of the perturbation differ in the various cases? The specific questions that this study aims to answer are: what is the vertical structure of the perturbations and how does it evolve in time; why do certain modes preferentially occur in certain years or months; how do baroclinic vs. barotropic processes contribute to the growth; and is the relative location of the AEJ and TEJ a critical but indirect factor in wave growth or decay via the enhancement or suppression of vertical motion?

It should be noted that we do not consider the origin of the perturbation. Classically, the African easterly waves are assumed to be initiated by dynamical instabilities related to the AEJ (e.g., Burpee 1972). More recent studies, however, have concluded that dynamic instability alone is insufficient to initiate waves and that convection may play a role (e.g., Hall et al. 2006, Kiladis et al. 2006). Convection, in turn, is frequently triggered by orographic effects (e.g. Mohr and Thorncroft). Thus, the waves often develop near highlands such as Darfur (e.g., Mekonnen et al. 2006), Tibesti, Aîr (Baum 2006) or the Hoggar (Reed et al. 1988). Our work merely follows the evolution of a perturbation introduced into a flow similar to that prevailing over West Africa. Only dry dynamics are considered. Thus, feedbacks between convection and the basic state cannot be considered. However, the extent to which simulated waves resemble observed waves provides some insight into the importance of dry dynamics in producing the interannual variability of rainfall over West Africa.

This paper begins in section 2 with a review of the meteorology of the Sahel, including the precipitation anomalies of the years evaluated. The model and the basic state are described in section 3. The results of the simulation are presented in section 4. Section 5 considers relevant issues, such as the contrast between wet and dry years, the role of wind shear, the impact of waves and convection on the mean basic state, and the relationship between the AEJ and the TEJ.

2. Overview of the meteorology of the Sahel

2.1 Rainfall Variability

Rainfall variability in sub-Saharan West Africa is characterized by a high degree of spatial coherence, such that two basic spatial patterns (Fig. 2) describe most of the rainfall variability on both seasonal and interannual time scales (Nicholson 1980, 1981, 1986, Janowiak 1988, Janicot 1992a, Nicholson and Palao 1993, Moron 1994, Fontaine et al. 1995, Ward 1998). The most common is essentially a dipole (Fig. 2, bottom patterns). Rainfall anomalies of the opposite sign prevail in equatorial and subtropical sectors (i.e., the Guinea Coast vs. the semi-arid Sahel). The node of the dipole is rather persistently around 10 ^{o} N. Anomalies of the same sign throughout these regions characterize the second pattern, termed no-dipole. The dry phase of this pattern (top right pattern, ubiquitously dry) is very common but the wet phase (top left pattern, ubiquitously wet) occurs infrequently.

We have developed a framework for analyzing rainfall variability that is based on a hypothetical link between these patterns and the African Easterly Jet (Fig. 2) (Nicholson and Grist 2001, Nicholson 2007b). In this framework, the dipole patterns are manifested mainly by factors influencing the **position** of the tropical rainbelt, while the no-dipole patters are manifested by factors influencing its **intensity**. A displacement of the AEJ is also evident in the dipole patterns, but that the AEJ remains close to its mean position when either of the no-dipole patterns prevails (Fig. 2).

Nicholson and Grist (2001) noted two relatively stable positions of the AEJ, termed the "Sahel" track and the "Guinea Coast" track (Fig. 2). In the former the jet lies in a more poleward

position over the Sahel, with its core at roughly 15 ^{o} N during the months of June through September. This produces the wet phase of the dipole (Sahel wet/Guinea Coast dry). In the "Guinea Coast" track the jet lies further equatorward, to the south of the Sahel, with its core at roughly 10 ^{o} N.

The no-dipole patterns are clearly distinguished on the basis of the intensity of the rain-producing mechanism. This is based on the rainfall rate in the core of the rainbelt and the magnitude of vertical motion associated with the rainbelt. An anomalously weak rainbelt results in the ubiquitous negative rainfall anomalies of the no-dipole pattern. An intensification of the rainbelt results in the ubiquitous positive anomalies. The core of the rainbelt is at roughly 10 ^{o} N in both cases.

2.2 The circulation over West Africa during the "summer" season

Fig. 3 shows a vertical cross-section of mean zonal winds over West Africa during August. Key features include the African Easterly Jet (AEJ) at ~ 650 mb, the Tropical Easterly Jet (TEJ) at ~ 200 mb, the upper-tropospheric westerly jets of both hemispheres, and the low-level westerly "monsoon" flow lying to the north of the equator. Grist and Nicholson (2001) showed that the contrast between wet and dry years was most evident in the strength of the TEJ, the latitudinal position of the AEJ, and the degree of development of the low-level westerly flow. In some months a second mid-level easterly jet develops south of the equator. Nicholson and Grist (2002) used the terms AEJ-North and AEJ-South to distinguish the two jets.

In the wet years (left hand side of Fig. 3) the TEJ was markedly stronger and the AEJ was situated about five degrees further north than in the dry years (right hand side of Fig. 3), and the

westerlies extended well into the mid-troposphere and were quite intense. Over West Africa as a whole, vertical and horizontal shear were substantially stronger in the wet years than in the dry years, indicating stronger barotropic and baroclinic instability in the wet years. The baroclinic effect was particularly strong in the Sahel. This was a consequence of the northward shift of the AEJ into Sahelian latitudes in wet years and its position south of the Sahel in dry years. This meant that the associated vertical shear and baroclinic instability were important in the Sahel in wet years, but completely absent in this region in dry years.

2.3 Mesoscale and Synoptic Systems Influencing West Africa

In West Africa the dominant convective system is westward-propagating mesoscale disturbances, termed cloud clusters. Environmental factors such as buoyant energy and wind shear determine whether isolated convection is turned into these long-lived and organized systems (Laing and Fritsch 1993). The frequency of cloud clusters and the amount of rainfall associated with them are modulated by transient synoptic-scale African or easterly waves (Houze and Betts 1981; Thompson et al. 1979). These waves, which have a typical wavelength of 2500 km, traverse the tropical latitudes of West Africa every 3 to 6 days (Avila and Clark 1988). The link between the waves and cloud clusters and or squalls appears to be limited to the later months of the season (Reeves et al. 1979; Chen and Ogura 1982; Miller and Lindzen 1992). The waves are also an important factor in the generation of squall lines, especially at this time (Fink and Reiner 2003).

For the waves to organize rainfall, they must produce moisture convergence. This requires that they be reasonably close to the moist layer. Past studies have suggested that in the Sahel, these prerequisites are present only in late summer. This fact may help to explain the

strong contrasts in the rainfall regime of June-July vs. August-September (Nicholson and Palao 1993) and the fact that mesoscale convective complexes are much more frequent later in the season (Laing and Fritsch 1993), when wave amplitude is larger (Duvel 1990). Grist (2002) and Grist et al. (2002) demonstrated that contrasts in wave activity appear to be critical factors in modulating rainfall on interannual timescales.

It has long been accepted that the African Easterly Waves (AEW) originate as a consequence of a joint baroclinic-barotropic instability associated with the vertical and horizontal shear of the AEJ. More recent papers (e.g., Hall et al. 2006) have suggested that the dynamic instability, while important in wave development, cannot initiate the waves. The AEWs are generally confined to a relatively narrow latitudinal zone near and south of the jet (Laing and Fritsch 1993; Norquist et al. 1977; Albignat and Reed 1980; Burpee 1972). Tourre (1981) and Bounoua (1980) noted that the waves are generally limited to a region lying between the axes of the AEJ [-North] and the TEJ. Nicholson and Grist (2001) further showed that the cores of the AEJ-North and AEJ-South straddle this region.

The growth and development of the waves are influenced by several factors, including Saharan dust (Karyampudi and Carlson, 1988), the magnitude of the horizontal and vertical shear of the AEJ (e.g., Rennick, 1981), and latent heat release (Norquist et al. 1977). A number of general circulation models have successfully simulated the waves (Reed *et al*., 1988; Druyan and Hall, 1994, 1996; Xue and Shukla, 1993; Thorncroft and Rowell 1998). Both observations and models have shown that characteristics of the AEJ (particularly horizontal and vertical shear) and the mean zonal flow influence the characteristics of these waves (Burpee, 1974; Simmons, 1977; Mass, 1979; Rennick, 1976, 1981; Kwon, 1989).

2.4 Rainfall in the Years 1950, 1955, 1983 and 1984

The rainfall anomaly patterns corresponding to the June-September season for the years 1950, 1955, 1983 and 1984 are shown in Fig. 4. The data are taken from the African precipitation data set compiled by the P. I. (e.g., Nicholson 1986, 2007b). These years represent the four anomaly configurations shown in Fig. 2. They were chosen based on the magnitude and spatial consistency of the anomalies. The same years are utilized as case studies in a series of analyses (e.g., Nicholson 2007a, b). Typically the anomaly is defined with respect to a departure from the mean and then "standardized" by dividing by the standard deviation. This is done on a station-by-station basis and the so-derived anomalies for stations within each region are then averaged. The anomalies are calculated with respect to the mean for the 30-year period 1968-97.

The years 1950 and 1955 were clearly very wet in the Sahel in the boreal summer and 1983 and 1984 were very dry. For the zone as a whole rainfall averaged 750 mm in 1950, compared to less than 250 mm in 1983 and 1984. There is a pronounced dipole in the years 1950 and 1984 that is evident for the three-month season and for August anomalies. Throughout West Africa, seasonal rainfall anomalies are positive in 1955 and negative in 1983.

Fig. 5, showing contours of rainfall as a function of month and latitude, serves to depict the intensity of the rainbelt over West Africa. The monthly rainfall rate at the core of the rainbelt is an indicator of intensity. This core generally lies somewhere between 7 ^{o} N and 12 ^{o} N during the June-to-September season (note that the intense rainfall around 5 to 6 ^{o} N has a more local origin). The intensity is high in both 1950 and 1955, but in 1955 the rainbelt lies much further south during the June-to-September season. In the core, rainfall exceeds 250 mm/mo. The reduced intensity is striking in 1983, with rainfall in the core being on the order of 150 mm/mo.

In 1984, when the Sahel is exceedingly dry and the Guinea Coast is relatively wet, the belt is relatively intense but remains anomalously far south most of the year.

3.0 The Model

3.1 Model Characteristics

The numerical model used in this investigation was kindly provided by Dr. J. S. Whitaker, of CDC NOAA, who developed the model during the course of his research. It is a primitive equation spectral model (Peng and Whitaker 1999) expressed in spherical coordinates. In this study the model is used in the linearized context with a zonally-invariant basic state derived from observed data on dynamical flows prevailing over West African in the longitude belt 10W-10E during specific months and years.

The model's basic states are constructed from observed data interpolated at the pressure levels of the model. The model is adiabatic and consists of three prognostic equations: the vertical velocity-, the divergence- and the thermodynamic- equations along with two diagnostic equations, the continuity equation used to compute the vertical motion in p-coordinates and the hydrostatic equation used to compute the geopotential. Horizontal hyper-diffusion is imposes a damping time of 6 hours on the smallest resolved horizontal scales. At T32 the model contains 32 waves and the grid size in the zonal and meridional direction is about 3.7 degrees of latitude/longitude with a 48x96 grid lattice for latitude and longitude. Numerical experiments for August 1950 and 1955 were performed at T32 with a 20 p-level model and a 4 p-level model. The results of the two models were similar. The 4-level model was retained for its simplicity and

in the hope of obtaining, in future papers, analytical results that could be compared with the numerical experiments.

In the 4-layer model the momentum Rayleigh friction is imposed on the 875mb level and at that level the damping time scale is taken to be 2.9 days. The coefficient of friction utilized was 1.42 E-11. Valdes and Hoskins (1989) and Hoskins and Karoly (1981) showed that at mid-latitudes, one can adjust the value of the constant Rayleigh friction to mimic a vertical velocity that is reminiscent of the Ekman layer vertical velocity. A follow-up study by Thorncroft and Hoskins (1994) found the wave growth to be relatively insensitive to the distribution of damping. Investigating the dynamics of moist Kelvin waves on a tropical beta plane, Wang (1988) derived a barotropic lower frictional layer designed for equatorial conditions; the vertical velocity at the top of such a layer is a function of the latitude as well as the parameter of the perturbed flow. The use of this frictional layer in the dynamics provided numerous physical results that will be re-examined.

To separate the West African region from mid-latitude regions, lateral sponge layers are imposed at latitudes ± 38 degrees and extend on both sides of the equator at all levels to the respective pole. The diffusion coefficient was increased linearly with latitude so that the waves entering the sponge layers will be gradually dissipated. The sponge layer is the same for both momentum and temperature fields.

3.2 Model Solution

Once the u (y, p) background state is selected (see 3.3), the numerical model is integrated forward in time using standard spectral techniques with numerical calculations performed alternatively in grid space and wave number space. The initial condition consists of inserting at

17 ^{o} N a barotropic vortex with a radius of 1500km. In the vortex the maximum zonal wind is 9 ms^{-1} at a radius of 700km and outside the initial vortex the perturbations are zero.

The latitude 17 ^{o} N was chosen as it represents the central Sahel. It is also roughly corresponds to the northern track of easterly waves (Reed et al. 1988, Baum 2006). The size of the initial vortex is the same order of magnitude as convective and topographic features over West Africa (Ali et al. 2003, Ricciardulli and Sardeshmukh 2002) and comparable in size to many cloud clusters. The magnitude of the perturbation is also comparable to the maximum meridional wind in some easterly waves (Thorncroft and Hoskins 1994). Sensitivity studies were conducted in which the perturbation size and magnitude were independently halved. The impact on the results was minimal, suggesting that in the dry case wave development is controlled by the characteristics of the basic state rather than those of the initial perturbation.

Because the model's architecture resembles that of GCMs the perturbations are started from an initial disturbance consisting of an initial barotropic vortex and integrated forward in time. Its growth rate is calculated from total kinetic energy. This rate is computed at every time step, hence several times per day. The integration proceeds for 60 days, roughly the equivalent of the waves circumscribing the earth in a uniform atmosphere with the background state as observed over West Africa. In this problem we are interested only in wave behavior over a limited area, the some 5,000 km of West Africa. For that reason, the growth rates discussed in section 4 are those obtained at day 6 of this linear integration, roughly corresponding to a distance of 5,000 km.

The manner in which these growth rates are obtained differs from the normal mode method used in our previous investigations (Grist et al. 2002) in which a quasi-geostrophic channel flow model was used with a zonal basic state centered around 15 ^{o} N. The normal mode

approach assumes that the solution is separable in space and time. The time factor of that solution contains the phase speed that is an eigenvalue associated with a given eigenfunction of the flow. The solution of this eigenvalue problem provides a dispersion relation, from which one obtains and displays the growth rate as a function of wavenumber or wavelength. The current model depicts considerably more specific detail of the dynamical processes. Its spectral construction permits evaluation of the temporal evolution of individual wavelengths in both the vertical and horizontal directions. The model also allows for the quantification of the baroclinic and barotropic processes involved in the growth.

3.3 Deriving the Basic State

The basic state is constructed from NCEP/NCAR reanalysis atmospheric data (Kalnay et al. 1996) obtained in the swath of longitudes between 10 ^{o} W and 10 ^{o} E and extending in latitude from pole to pole. The zonal flow and zonally-averaged potential temperature for certain months of certain years characterize given basic states that extend around the globe in spherical coordinates centered at the equator. We focus on the tropical band centered at the equator and bounded at 39 degrees of south/north latitude.

The selection of the data in the longitude band 10 ^{o} W-10 ^{o} E ensures that in the basic state flow occurs over a zonal land mass bordered at its southern edge by a zonal water mass as a paradigm for West African flows. The temperature contrasts between the ocean, around 5 ^{o} N, and the Sahara, around 25 ^{o} N are among the important dynamical ingredients that drive these flows. The longitude of 10 ^{o} W was selected to free the basic sates from local effects of the

Atlantic edge and the choice of the longitude of 10 ^{o} E frees these basic states from the edge effects arising from the African landmass that extends south past the equator.

Hall et al. show that dry wave characteristics are sensitive to zonally varying basic states. However, the basic state in which the waves grow over West Africa does not show strong zonal asymmetries. For example, there is little contrast between the mean basic state for 10 ^{o} W to 10 ^{o} E and for 10 ^{o} E to 20 ^{o} E (Nicholson and Grist 2003). Even in individual years the symmetry is relative strong throughout this sector. Hence the zonally invariant basic state in the model is representative of realistic conditions. Also, it is appropriate for perturbations initiated anywhere within this sector.

3.4 Zonal winds and zonal potential temperature fields.

Fig. 6 shows the basic state zonal wind for the summer months of the years 1950, 1955, 1983, and 1984. This figure contains interesting features that impact the dynamics. We observe that the Tropical Easterly Jet (TEJ) is much weaker in the dry years than in the wet years. In fact, the TEJ is barely evident over this region of Africa in the dry years. The opposite is true for the AEJ. It is strong and well developed in the dry years but weak and latitudinally constricted in the wet years. The AEJ is located around 10 ^{o} N in the dry years but closer to 15 ^{o} N in the wet years (particularly in 1950), but the core of the TEJ is relatively invariant from year to year and located at roughly 10 ^{o} N in July and August. The result is that the jet axes are aligned during the dry years but in the wet years the AEJ axis is several degrees poleward of the TEJ axis. In the dry year 1984 both the AEJ-North and the AEJ-South are well developed in September. These jets

straddle the equator. The low-level monsoon flow is also different in the wet and dry years, being much shallower in the latter. It is particularly deep and strong in 1950. The result is strong vertical and horizontal shear in the wet years.

The wet and dry year configurations of the three major features, the TEJ, the AEJ and the monsoon flow, affect the dynamics in several ways. The most obvious is in the shear. The stronger horizontal and vertical shear in the wet years suggests that both barotropic and baroclinic instability are stronger in the wet years than in the dry years. The alignment of the axes affects the relative juxtaposition of the convergence and divergence zones associated with the "jet streaks" of the cores and the areas of cyclonic vorticity on the equatorward flanks of the two jets. The depth of the monsoon flow also potentially affects the penetration of moisture to the level of the AEJ.

The basic state potential temperature is shown in Fig. 7. The Sahara north of ~ 25 ^{o} N and the Atlantic Ocean south of ~ 5 ^{o} N provide the warm and cold reservoirs controlling much of the dynamical behavior in this region. Only 1950 is shown because there is little contrast among the four years. The strong meridional potential temperature gradients near the ground indicate the regions where strong vertical shears are likely found near the ground. In the 1984 these gradients were somewhat weaker than in the other three years.

4.0 Results

The model provides a picture of the horizontal and vertical structure of the waves, the growth rate as a function of time and the growth rate as a function of wave number on each day of simulation. Although the model runs extended for 60 days, all results are examined here for

day 6. By this time, the wave characteristics had stabilized and in the wet years exponential growth had begun. The spatial picture of the waves from 39 ^{o} N to 39 ^{o} S is examined at four levels (875, 625, 375 and 125 mb), then vertical profiles are described for latitudinal cross-sections at 17 ^{o} N and 13 ^{o} N. The two latitudes represent the central and southern Sahel. The 625 mb and 125 mb levels, respectively, are representative of the AEJ and TEJ. The results for June and July are described separately from August and September because different dynamic factors appear to be operative in the two sets of months (Nicholson and Palao 1993).

4.1 Growth rate

The growth of the maximum north-south perturbation for August (the wettest month) is shown in a log plot of wind speed as a function of model time in Fig. 8. The August growth is depicted for the wet year 1955, the wet dipole year 1950, the dry year 1984 and the dry dipole year 1983. In the wet years perturbations decay in the first few days of integration then grow exponentially. In the dry years there is likewise initial decay. Decay continues in the case of 1984, but in 1983 weak growth is maintained.

We have arbitrarily selected day 6 as the time at which exponential growth rate is achieved and the growth rates for individual wavelengths were obtained from model data at model-day 6. As indicated, this is deemed appropriate for evaluation of wave development over a limited spatial area, i.e., the western portion of North Africa. Growth rates were calculated as half of the time rate of change of the logarithm of the kinetic energy of each wave mode over the entire domain. Fig. 9 shows unstable wavelength bands and growth rates vs. wavelength

expressed in km for the months of June through September for each of the four years. The figure displays only growth rates exceeding -0.1 day^{-1}.

In the dry years the perturbations are substantially damped, although some scales of motion attempt to grow sporadically over the integration time, never quite achieving positive growth rates. That is the case for all months of 1984 and for June and September of 1983. In July and August of 1983, growth rates on the order of .05 day^{-1} are reached for a band of wavelengths centered around 3700 km. The strongest growth extends over a broader band for August than for July.

In the wet years the perturbations grow more vigorously and the strongest growth falls within a wide, unstable wavelength band that varies with year and month. The wide and fairly flat band of unstable wavelengths implies that wave groups are likely to be present. The growth rate as a function of wavelength shows an inverted parabolic-shaped peak around 3000 to 4000 km, depending on year and month, and a cutoff around 5000 km. In all years and months strong positive growth rates are achieved. For 1950 strong positive growth rates, reaching .1 to .15 per day, are evident for all months, but they are somewhat weaker in July. Peak growth is at about 3500 to 4000 km in July and August but 3000 to 3300 km in June and September. In 1955 growth rates exceeding 2 day^{-1} are reached in both July and August, with peak perturbation growth at about 3300 km. Unstable rates are indicated for a band ranging from around 2500 km to 5000 km. These greatly exceed the growth rates during the same months in 1950. Growth rates are considerably lower for June and September of 1955.

The growth rates of 1950 show an interesting feature. In July, August and September the maximum growth rate is around 3500 to 4000 km and a well-defined cut-off is seen around 5000 km. However, there is also a tendency for longer waves again around 6000 km or 7000 km. This suggests that both synoptic scale and planetary scale waves are active in the rainy season of some

particularly wet years. The second band of unstable waves is also apparent in August of 1955, beginning at about 7300 km.

A comparison of the individual months is also interesting. In June, instability is evident only in the two wet years. In July and August instability is evident in all years except 1984. In both months the greatest instability is in the year 1955. The main difference between July and August growth rates are the rate of the growth in 1950, which was markedly lower in July than in August. The main difference between July and August is apparent only for 1950. In September, as in June, the greatest instability is evident for 1950.

The weaker growth rate for 1950 than for 1955 is interesting, in light of the comparable rainfall totals in the Sahel. Noteworthy is that the contrast in model growth rates is most apparent at the shorter wavelengths, particularly from about 2500 km to 4000 km. Also, a sharp peak is apparent in 1955 at about 3000 km to 3300 km. This implies that there may have been a larger number of relatively shallow disturbances in 1955 compared to 1950.

4.2 Vertical Structure of the Waves

The waves are depicted in Figs. 10 through 13 for the years 1983, 1984, 1950 and 1955, respectively. The stream function and mean zonal wind for latitudes 17 ^{o} N (where the vortex was introduced) and 13 ^{o} N are shown in the second set of panels. A comparison of the four figures shows that the waves are, in general, much more strongly developed in the wet years than in the dry years. The waves are particularly weak throughout 1984. The reduced wave activity in 1983 and 1984 is evident in all four months, but the strongest contrast is for the months

of August and September. Notable differences are also evident between the two dry years and between the two wet years.

4.2.1 June and July

In June of 1983 and 1984 the waves are weak and confined to the lower and mid-troposphere (Fig. 10a and b). Some waves are apparent at the TEJ level but they appear to be dissociated from those of the troposphere. The waves exhibit a baroclinic structure below and above the level of the AEJ, especially at 13 ^{o} N. Compared to June 1983, the waves in June 1984 are markedly weaker and more vertically limited. Also, the wave maximum is generally near the surface in 1984, but several waves have a maximum at the AEJ level in 1983.

In June of 1950 the waves are intense and extend to the upper troposphere, but not to the TEJ level (Fig. 10d). The maximum is near the surface but the waves are well developed and strong near and above the AEJ. The structure is baroclinic below the AEJ but barotropic above. The wave structure in June, 1955 (Fig. 10c), is similar to that in June, 1983. The waves are more intense in 1955, but the same degree of vertical development is evident in both years. At both latitudes the waves are baroclinic below the AEJ, but barotropic or weakly baroclinic above.

In July of 1983 and 1984 the waves are overall markedly stronger than in June and strong waves are also apparent up to the TEJ level (Fig. 10a and b). The wave maximum is generally near the surface, but several waves have a maximum at the AEJ level, especially at 13 ^{o} N. Contrasts are apparent in the wave structure in 1983 and 1984. The strongest waves are confined to the lower troposphere in 1983, and are dissociated from the waves at the TEJ level, while the

wave packets extend from the surface to the TEJ in 1984. In 1984 the waves are baroclinic at and above the AEJ level but in 1983 the waves are predominantly barotropic.

In July the waves were stronger in 1950 and 1955 (Figs. 10c and d) than in 1983 and 1984. In both years, the wave maximum was near the AEJ level and the wave structure was barotropic. In 1950 the waves extend to the TEJ level and appear to propagate upward from the surface. In 1955 the waves were confined to the mid- and lower troposphere and were stronger than in 1950.

4.2.2 August and September

The waves of August and September in the wet years 1950 and 1955 contrast strongly with those in the two dry years in terms of strength, vertical development and instability (Figs. 12 and 13). As was the case in June and July, the waves of August and September are more intense during the wet years than the dry years. Wave activity is particularly weak in September of the two dry years. In the dry years the waves also tend to be baroclinic and best developed near the surface. In the wet years the waves tend to be barotropic and most intense near the level of the AEJ. In the dry years the waves tend to reach the upper troposphere but not to the level of the TEJ. They extend from the surface to the TEJ level in August and September of the wet years.

August 1983 and August 1984 are similar: the waves are moderately strong waves and generally have a baroclinic structure both below and above the AEJ. The wave maximum lies near the surface in most cases and the waves usually extend from the surface to 300 mb or 350 mb. A few waves are evident near the TEJ level but appear to be dissociated from the lower-level waves. In August of 1950 and 1955 the waves are strong, generally barotropic and generally have a maximum near the AEJ level. The main contrast between Augusts of the two years is that the waves are stronger in August of 1955.

The same contrasts between wet years and dry years are evident for September. Also August and September are fairly similar, except that in the dry years the waves are markedly weaker in September than in August. Two contrasts are to be noted. For one, the wet years, in the upper troposphere the waves are stronger in August than in September. However, in both months the wave structure is predominantly barotropic in the wet years. Secondly, in the dry years, the waves structure in the upper troposphere is different in the two months. In both cases, the wave structure is baroclinic below the AEJ, but can be baroclinic or barotropic above.

4.3 Horizontal Structure of the Waves

The bottom two sets of panels in Figs. 10 through 13 depict the horizontal structure of the waves at each model level: 875, 625, 375 and 125mb. The main contrasts in the horizontal structure of the waves are the latitudinal extent and location of the core of the wave. In most cases, the waves in the lower and mid-troposphere are best developed in the subtropical latitudes of the northern hemisphere and generally restricted to these latitudes.

In June some extend across the equator into the Southern Hemisphere. The cross-equatorial extent is particularly apparent at higher levels. The strongest contrast in horizontal structure between June of wet and dry years is that the wave maximum at 375 mb is in the southern hemisphere in the dry years. The wet and dry years show somewhat more contrasts in the intensity of the waves in June. However, this contrast is still relatively small. This fact is noteworthy because the contrast in precipitation in these years in also relatively small in June.

In the remaining months the waves tend to be restricted to the northern hemisphere in the low and mid-troposphere but become cross-equatorial in the upper troposphere. In all three months the most apparent contrast between the wet and dry years is the latitudinal extent of the

waves at the AEJ level (625 mb) and the TEJ level (125 mb). In the wet years waves near the AEJ extend across the equator but at the TEJ level the waves are concentrated in the Northern Hemisphere. In the dry years waves near the AEJ are confined to a comparatively small latitudinal band and are restricted to the Northern Hemisphere while waves at the TEJ level show strong cross-equatorial development and are sometimes most strongly developed in the Southern Hemisphere.

5.0 Discussion

5.1 Wet and Dry Year Contrasts

To facilitate the synthesis of results, various characteristics of the waves are summarized in Table 1. This includes wave strength (difference between the maximum and minimum of the stream function in the appropriate month of Figs. 10-13), the levels where the waves are evident, the vertical location of the wave maximum, the number of waves at the AEJ level, the instability suggested by the wave structure above and below the AEJ level, the coupling between the waves at the AEJ and TEJ level, and the shear between 875 and 125 mb.

Two consistent contrasts between the wet and dry years are apparent. The waves are markedly stronger in the wet years. They also show a barotropic structure throughout the troposphere. The only exception to the latter is the baroclinic structure in June of the wet years below the AEJ level. Also evident is that during August and September of the wet years the waves tend to be best developed at the AEJ level. In June, July and August the waves tend to extend throughout the troposphere to the TEJ level in the wet years, but not in the dry years. The only exception is July of 1984.

These results compare well with the observational analyses of Grist and Nicholson (2001) and Grist (2002). The latter study contrasts ten wet years with ten dry years. Our two dry years 1983 and 1984 are included in his dry composite but our two wet years are not included in his wet composite, as his analysis commenced with the year 1958. Grist's analysis was also restricted to the 925 mb and 600 mb levels. However, the basic conclusions of our work are in agreement with his. The most notable findings are the stronger waves and the stronger barotropic instability in the wet years (see Fig. 14). He also found more waves in the wet years. Our results are consistent with this observation. There are generally three or four waves in all four months of the dry years. In the wet years there are seven waves in July and August, four to six in June and September.

5.2 The Role of Wind Shear

An important feature is evident in the basic states corresponding to the four years: the much stronger shear throughout the troposphere in the wet years (Figs. 10 to 13). The upper tropospheric shear appears to be a key factor in determining wave development in the wet years. The weak overall shear suppresses the vertical development and the waves instead extend well across the equator and into the southern hemisphere. This shear is dependent on the intensity of the TEJ. When the TEJ is weak, a strong layer of weak or westerly shear just above the AEJ appears to restrict the vertical development of the waves. Xie and Wang (1996) provide an explanation for this effect. In the presence of an Ekman boundary layer, easterly shear favors Rossby wave instability more than westerly shear because of a combined effect of the boundary layer Ekman pumping and vertical shear. In the case of easterly/westerly shear, the phase shift between the barotropic meridional wind and the thickness tends to favor/suppress the

conversion of potential energy from the mean flow to eddies. Xie and Wang suggest that the probable reason is the contrast between wave structure and surface friction-induced moisture convergence in the two cases.

Westerly or weak easterly shear is clearly apparent above the AEJ in the months of July and August 1983. The model results show stark contrast with the same months of the wet year 1950. In 1950, a small number of extremely intense waves develop at the TEJ level (two in the case of August 1950). These are restricted to a relatively narrow latitudinal zone, but they are clearly associated with waves extending from the TEJ level down to the surface. This situation is interesting because of a characteristic of the rainy season noted by several authors (e.g., Lamb et al. 1998, Nicholson 2000, and Le Barbé et al. 2002): the difference between a dry and a wet August is not seen in the number of disturbances but in the presence of one or two disturbances that bring tremendous amounts of rainfall.

We speculate that the vertical and horizontal structures of the basic state for August 1950 are factors in such intense events. This is tested with an observational analysis, based on NCEP Reanalysis Data. Fig. 15 shows filtered meridional wind at 10 ^{o} E from the surface to 125 mb during August 1950. There are two intense waves with a maximum near the TEJ level. Daily rainfall at Maradi (7 ^{o} E) within the time of the wave passage was 137 mm for the wave on August 5/6 and 100 mm for the wave on August 18/19. This is nearly 50% of the mean rainfall for the month of August. Overall rainfall at Maradi was extraordinary throughout August 1950. Daily rainfall exceeded 75 mm on five days; typically the maximum daily rainfall in August is 30 mm to 40 mm. Comparable daily totals occurred on only two other occasions during the period 1934 to 1965, with 76 mm in August 1938 and 86 mm in August 1956.

5.3 The impact of wave activity and convection on the basic state

This study relies on observed contrasts between wet and dry years in the Sahel, years that differ in terms of the intensity of wave activity and convection. In particular, the development of waves from the mean flow can weaken the zonal mean. On the other hand, convection might enhance it. This leads to the question of how much of the contrast in zonal winds between wet and dry years might be a result of wave activity and convection. Several arguments suggest that is not the case.

As for the waves, two points of reasoning suggest that the mean zonal speed at the AEJ level might be on the order of 3 m s-1 or less. One is that that maximum meridional perturbations associated with the waves are on the order of 5 to 8 m s^{-1}, although waves with meridional maxima as great as 10 m s^{-1} are not uncommon (Reed et al. 1977, Thorncroft and Hoskins 1994, Hall et al. 2006). Since there is significant wave activity on roughly one half to two-thirds of the days within the wave season (Grist 2002), the reduction would be less than 3 to 5 m s^{-1}. Thorncroft and Hoskins (1994) found that the growing waves weakened the jet maximum by only 3 m s^{-1}.

This value more or less represents an upper limit to the degree to which weakening of the zonal flow by waves might explain the contrast between the AEJ strength in wet and dry years. However, there is still significant wave activity in the dry years. Grist (2001) found that the number of days with significant wave activity in dry years was roughly two-thirds of the number in wet years. This would indicate that the waves account for a contrast in zonal speed of the AEJ on the order of 1 ms^{-1}.

That is roughly half the contrast in the speeds between the wet and dry years examined. However, the contrast in speed is apparent well before the wave season (Grist and Nicholson

2001). Also, the AEJ speed is dictated not only by thermal wind considerations but also by the flow upon which the shear is imposed. This is considerably different in the wet years, with the well developed equatorial westerly maximum, and the dry years. Perhaps more importantly, the shear and not the AEJ speed is the critical factor that differs between wet and dry years. This is not greatly impacted by the AEJ core speed, since that speed varies by only a few ms^{-1}.

As for the wet-dry contrast in TEJ speed, wave activity generally extends to the TEJ level only in wet years, when the TEJ speed is greatest. Hence, waves do not weaken the TEJ. Redelsperger et al. (2002) suggest that convection can increase upper-level shear via latent heat release. This effect cannot account for the contrasts in maximum TEJ speeds between the wet and dry basic states simulated by our model. This contrast is as large as 20 ms^{-1}. For one, the stronger TEJ in wet years is evident prior to the season of intense convection over West Africa. More importantly, "wet" and "dry" refer to the rainfall anomaly in the Sahel and not the intensity of convection. The intensity of convection is equally strong in the 1950, when the speed of the TEJ core exceeded 30 ms^{-1}, and 1984, when its core speed was on the order of 12 ms^{-1}. Thus the contrast in the basic state between the wet and dry years in the Sahel is not due to contrasting convection in these sets of years.

5.4 Relationship between the AEJ and TEJ

Overall the importance of a link between the AEJ and TEJ during the wet years appears to be well established from our results. Analysis of the dynamical links goes beyond the scope of this work. However, other analyses suggest several associations. For one, the presence of a strong TEJ enhances the shear near the AEJ, thereby generally increasing the instability and allowing waves to develop vertically. Also, associated with the TEJ is a strong region of

divergence (Nicholson 2007b) that promotes ascent in the lower and mid-troposphere. This further entrains the low-level moisture into higher levels, well into the vicinity of the AEJ. This is relevant, as moisture near the jet is a prerequisite for the waves to organize isolated convection into mesoscale systems that bring intense rainfall.

Potential vorticity (PV) theory suggests further ways in which interaction may take place. Two results are of particular importance in this context. The first is that the model produces two types of waves of very different wavelengths (planetary and synoptic scales) during certain months and years. The second is that the planetary scale waves are seen only at the TEJ level (viz. Fig. 12).

Over West and Central Africa there are three reservoirs of PV: the surface, the AEJ, and the TEJ. The surface is involved because surface temperature plays the same role as PV. Each reservoir supports PV waves and the north-south PV gradients of the PV distributions conspire with the beta effect to control the propagation of the PV waves on these reservoirs (Barcilon and Bishop, 1999). These waves communicate with each other when their penetration depth equals or exceeds the vertical distance between two PV-reservoirs.

Three communication channels exist: AEJ-ground, AEJ-TEJ, and ground-TEJ. Each wave affects the other through this communication at a distance. Vertical structures then develop that evolve in time. The distances between the ground and AEJ and between the AEJ and TEJ are associated with the 3000-4000 km wavelength synoptic-scale waves. The distance between the ground and the TEJ (tropopause) level is associated with planetary waves. This crude picture, based on PV arguments, supports the observation of two bands of wave instability in flows over Africa. Further supporting evidence is that our preliminary initial value experiments showed that for the planetary-scale waves, wave growth begins on the TEJ and its amplitude propagates

downward. During the downward propagation, the planetary wave may contribute to the overall wave dynamics near the AEJ.

6.0 Summary and Conclusions

The model simulations show consistent contrasts between wave development in the wet and dry years and between the individual months of the rainy season. In the wet years, growth is characterized by initial dampening then exponential growth. In the dry years, the subsequent growth fails to materialize. Instability is greater in July and August than in June and September. It is evident in all years in July and August but only in the wet years in June and September. The wavelength of peak growth is also notably longer in July and August than in June and September, suggesting that shallower systems prevail early and late in the rainy season.

The model simulations also show consistent contrasts in wave characteristics in the wet and dry years. These are summarized schematically in Fig. 16. The waves are markedly stronger in the wet years and show a barotropic structure throughout the troposphere. During August and September the waves over North Africa tend to be best developed at the AEJ level in wet years but in the lower troposphere in dry years. In June, July and August the waves tend to extend throughout the troposphere to the TEJ level in the wet years, but not in the dry years. The upper tropospheric shear, which is stronger in wet years, appears to be a key factor in wave development.

This shear is dependent on the intensity of the TEJ, suggesting that the TEJ is an important factor in interannual variability in the Sahel region. When the TEJ is weak, a strong layer of anticyclonic shear just above the AEJ appears to restrict the vertical development of the waves. The weak overall shear further suppresses the vertical development. The result is weak wave

development over North Africa, with the waves instead extending well across the equator and into the southern hemisphere. This acts to suppress rainfall over North Africa. Although most waves appear to originate near the AEJ, some commence at the TEJ level and propagate downward.

Another contrast is that in the dry years the growth rates show a single maximum around 3,000 to 4,000 km, but in wet years there is a second around 6,000 to 7,000 km. This suggests that both synoptic scale and planetary scale waves are active in the rainy season of some wet years. Imposing considerations of potential vorticity, the generation of planetary scale waves implies a strong link between the surface and the TEJ in wet years. Such a link is absent in the dry years. This is likely a major factor in the interannual variability of rainfall in the Sahelian latitudes of West Africa. These planetary scale waves appear to be a factor in the huge waves that produce tremendous amounts of rainfall in some disturbances.

This study has answered many of the questions originally posed in Section 1. The perturbations generally appear in the mid-troposphere, although some appear at the TEJ level and propagate downward. The vertical shear determines why certain modes preferentially occur in certain years or months. Because the shear is determined by the relative location of the AEJ and TEJ, the latitude of these jets is a critical but indirect factor in wave initiation, growth or decay via the enhancement or suppression of vertical motion. Both baroclinic and barotropic processes contribute to the growth, but these differ from year-to-year and month-to-month. The contribution of both processes is often different above and below the AEJ level. The results are consistent with prior observational analysis. The gratifying correspondence between model results and past observational results is to be noted.

ACKNOWLEDGEMENTS

This work was supported by NSF grant ATM-0004479. We are much indebted to Dr. Jeff Whitaker, NOAA-CDC, who provided the linear GCM used in this study, and to NCAR, for providing the NCEP Reanalysis data. We would like to acknowledge the support for this research provided by the Geophysical Fluid Dynamics Institute of Florida State University. This is contribution No. xxx of the Geophysical Fluid Dynamics Institute at Florida State University. The third author would like to express his gratitude to Dr. C. A. Clayson, director of the Institute, for her support. Finally, we would like to thank FSU students Jeff Baum and Travis Smith for their assistance in the study and Prof. Phil Cunningham for valuable discussions and insights.

FIGURES

1. Rainfall in the Sahel 1901 to 2003, expressed as a regionally-averaged percent standard deviation (adapted from Nicholson 2005). The years used in this study are shaded: 1950, 1955, 1984 and 1983.

2. Conceptual model of rainfall variability sub-Saharan West Africa. Shading in the "rainbelt" indicates its core latitudes, with the degree of shading indicating intensity. Variations are a function of the intensity of the "rainbelt" and the latitudinal location of the AEJ, which determines the latitude of the rainbelt in the boreal summer. Changes in the intensity produce wet or dry conditions throughout, while shifts in the latitude of the AEJ produce the well-known rainfall dipole, with contrasting anomalies in the Sahel and

Guinea Coast. Large numbers on the maps indicate the analysis year corresponding to the pattern. Note also the reduced latitudinal extent of the rainbelt in the dry years.

3. Mean zonal wind speed (m s^{-1}) averaged between 20 ° E and 10 ° W for August (from Grist and Nicholson 2001). A composite of four wet years (1958-1961) is compared with a composite of dry years (1982-1985). Contours correspond to 2 m s^{-1}. Solid contours: westerlies; dashed contours: easterlies.

4. Regional rainfall anomalies for the June-to-September season for 1950, 1955, 1984 and 1983. Anomalies are expressed as a percent of the standard departure from the mean for the 30-years 1968-1997 (as in Nicholson 2007b).

5. Rainfall as a function of month and latitude at 0 ° W.

6. Mean zonal wind (m s^{-1}) of the basic state versus latitude for June through September of 1950, 1955, 1984 and 1983. Data are averaged between 10 ° W and 10 ° E; otherwise, as in Fig. 3.

7. Plots of zonally-averaged potential temperature profiles between ±31° latitude as a function of pressure from 875 mb to 125mb for June through September of 1950. The areas with potential temperatures of 310 - 315 ° K and 315 - 320 ° K are shaded. The data were selected in the band of longitudes between ±10 and the so-calculated basic state was extended around the globe. See text.

8. Wave growth vs. model day for August of the years 1950, 1955, 1984 and 1983.

9. Growth rates as a function of wavelength (in km) in June through September for the two wet years and two dry years. Wave growth rate vs. wave number on day 6; time shown is that corresponding to strongest wave activity during the day and varies with month and year.

10. Results for June. Top: vertical profile of the zonal wind (m s^{-1}) corresponding to the basic state. Center: Vertical profile of waves on day 6 as a function of longitude at the 17 ^{o} N and 13 ^{o} N. Bottom: wave activity as a function of latitude and longitude at four vertical levels (875 mb, 625 mb, 375 mb and 125 mb). Waves are expressed as the stream function (m^2s^{-1}), the magnitudes of which provide information on wave amplitude. The 0-contour is indicated in bold. To facilitate comparison of the four years, the maximum and minimum amplitudes of the stream function are indicated in boxes in the lower left of each frame. A longitude of 0 ^{o} corresponds to the longitude where the vortex was introduced and not the geographical longitude of 0 ^{o}. Note that only the longitudes from 135 ^{o} W to 135 ^{o} E are depicted; these longitudes are relative to the initial vortex.

11. As in 10, but for July.

12. As in 10, but for August.

13. As in 10, but for September.

14. Quasi-geostrophic potential vorticity gradient (x 10^{-11} s^{-1}), averaged between 10 ^{O} W and 20 ^{O} E at 15 ^{O} N and 600 mb as a function of the month of the year. Solid line is 40-year mean, short dashed line is for wet years and long dashed line is for dry years. (a) Total QGPV gradient, (b) barotropic term, and (c) baroclinic term (from Grist 2002).

15. Hoevmueller diagram of filtered meridional wind at 10 ^{o} E for August 1950 (averaged for 12.5 ^{o} to 20 ^{o} N). The filter retains periodicities on the time scale of 2 to 6 days (Nicholson et al. 2007). Data are from NCEP-Reanalysis.

16. Schematic of wet year and dry year waves. Major contrasts are the level of maximum wave development, the degree to which the waves are developed at 150 mb, and the extension of waves at 150 mb into the southern hemisphere in dry years.

Albignat, J.P. and R.J. Reed, 1980: The origin of African wave disturbances during Phase III of GATE. *Mon. Wea. Rev.*, 108, 1827-1839.

Ali, A., T. Lebel, and A. Amani, 2003: Invariance in the spatial structure of Sahelian rain fields at climatological scales. *J. Hydrometeor.*, 4, 996-1011.

Avila, L. A., and G. B. Clark, 1989: Atlantic tropical systems of 1988. *Mon. Wea. Rev.*, 117, 2260-2265.

Barcilon, A. and C. H. and Bishop, 1998: Nonmodal development of baroclinic waves undergoing horizontal shear deformation. *J. Atmos. Sci.*, 55, 3483-3597.

Baum, J. D., 2006: African easterly waves and their relationship to rainfall on a daily timescale. M.S. Thesis, Department of Meteorology, Florida State University, 170 pp.

Bounoua, L., 1980: Relation entre champ de vent, genese et propagation des lignes de grains ouest africaines. Memoire de fin d'etudes, I.H.F.R. Oran Algerie.

Burpee, R. W., 1972: The origin and Structure of Easterly Waves in the Lower Troposphere of North Africa. *J. Atmos. Sci.*, 29, 77-90.

Burpee, R. W., 1974: Characteristics of North African Easterly Waves during the summers of 1968 and 1969. *J. Atmos. Sci.*, 31, 1556-1570.

Chen, Y., and Y. Ogura, 1982: Modulation of convective activity by large-scale flow patterns observed in GATE. *J. Atmos. Sci.*, 39, 1260-1279.

Druyan, L., and T. Hall, 1994: Studies of African wave disturbances with the GISS GCM. *J. Climate*, 7, 262-276.

Druyan, L. M., and T. M. Hall, 1996: The sensitivity of African wave disturbances to remote forcing. *J. Appl. Meteor.*, 35, 1100-1110.

Duvel, J.P., 1990: Convection over tropical Africa and the Atlantic Ocean during northern summer. Part II, modulation by easterly waves, *Mon. Wea. Rev.*, 118, 1855-1868.

Fink, A. H., and A. Reiner, 2003: Spatio-temporal variability of the relation between African Easterly waves and west African squall lines in 1998 and 1999. *J. Geophys. Res.*, 108, 4332-4343.

Fontaine, B., S. Janicot, and V. Moron, 1995: Rainfall anomaly patterns and wind field signals over West Africa in August (1958-89). *J. Climate*, 8, 1503-1510.

Grist, J. P., 2002: Easterly waves over Africa. Part I: The seasonal cycle and contrasts between wet and dry years. *Mon. Wea. Rev.*, 130, 1337-1359.

Grist, J. P., and S. E. Nicholson, 2001: A study of the dynamic factors influencing the interannual variability of rainfall in the West African Sahel. *J. Climate*, 14, 1337-1359.

Grist, J. P., S. E. Nicholson, and A. I. Barcilon, 2002: Easterly waves over West Africa II. Observed and modelled contrasts between wet and dry years. *Mon. Wea. Rev.*, 130, 212-225.

Hall, N. M. J., G. N. Kiladis, and C. D. Thorncroft, 2006: Three-dimensional structure of African easterly waves. Part II: Dynamical modes. *J. Atmos. Sci.*, 63, 2231-2245.

Hoskins B. J., and D. J. Karoly, 1981: The steady linear response of a spherical atmosphere to thermal and orographic forcing. *J. Atmos. Sci.*, 38, 1179-1196.

Houze, Jr., R.A., and A.K. Betts, 1981: Convection in GATE. *Rev. Geophys. Space Physics*, 19, 541-576.

Janicot, A., 1992: Spatiotemporal variability of West Africa rainfall. Part I: Regionalizations and typings. *J. Climate*, 5, 489-497.

Janowiak, J., 1988: An investigation of interannual variability in Africa. *J. Climate* 1: 240-255.

Kalnay, E., and Coauthors, 1996: The NCEP/NCAR 40-year reanalysis project. *Bull. Amer. Meteor. Soc.*, **77**, 437-471.

Karyampudi, V., and T. Carlson, 1988: Analysis of numerical simulations of the Saharan air layer and its effects on easterly wave disturbances. *J. Atmos. Sci.*, 45, 3102-3136.

Kiladis, G. N., C. D. Thorncroft, and N. M. J. Hall, 2006: Three-dimensional structure of African easterly waves. Part I: Observations. *J. Atmos. Sci*., 63, 2212-2230.

Kwon, H.J., 1989: A reexamination of the genesis of African waves, *J. Atmos. Sci.*, 46, 3621-3631.

Laing, A., and J.M. Fritsch, 1993: Mesoscale convective complexes in Africa. *Mon. Wea. Rev.*, 121, 2254-2263.

Lamb, P. J., M. A. Bell, and J. D. Finch, 1998: Variability of Sahelian disturbance lines and rainfall during 1951-1987. Water Resources Variability in Africa during the XXth Century (E. Servat et al., eds.), IAHS, Gentbrugge, Belgium, 19-26.

Le Barbé, L., T. Lebel, and D. Tapsoba, 2002: Rainfall variability in West Africa during the years 1950-90. *J. Climate*, 15, 187-202.

Mass, C., 1979: A linear primitive equation model of African wave disturbances. *J. Atmos. Sci*., 36, 2075-2092.

Mekonnen, A., C. D. Thorncroft, and A. Aiyyer, 2006: Analysis of convection and its association with African easterly waves. *J. Climate*, 19, 5405-5421.

Miller, R.L., and R. Lindzen, 1992: Organization of rainfall by an unstable jet with an application to African waves. *J. Atmos. Sci.*, 49, 1523-1540.

Mohr, K. I., and C. D. Thorncroft, 2006: Intense convective systems in West Africa and their relationship to the African easterly jet. *Quart. J. Roy. Meteor. Soc.,* 132, 163-176.

Moron V. 1994: Guinean and Sahelian rainfall anomaly indices at annual and monthly time scales (1930-1990). *Int. J. Climatology,* 14, 325-341.

Newell, R.E., and J.W. Kidson, 1979: The tropospheric circulation over Africa. In Saharan Dust (Scope Report 14), C. Morales, ed., Wiley and Sons, 133-170.

Newell, R.E., and J.W. Kidson, 1984: African mean wind changes between Sahelian wet and dry periods. *J. Climatology*, 4, 1-7.

Nicholson, S.E., 1980: The nature of rainfall fluctuations in subtropical West Africa. *Mon. Wea. Rev.*, 108, 473-487.

Nicholson, S.E. 1981: Rainfall and atmospheric circulation during drought periods and wetter years in West Africa. *Mon. Wea. Rev.*, 109, 2191-2208.

Nicholson, S. E., 1986: The spatial coherence of African rainfall anomalies: Interhemispheric teleconnections. *J. Clim. Appl. Meteor.,* 25, 1365-1381.

Nicholson, S. E., 1993: An overview of African rainfall fluctuations of the last decade. *J. Climate*, 6, 1463-1466.

Nicholson, S.E., 2000: Land surface processes and Sahel climate. *Rev. Geophys.,* **38**,117-139.

Nicholson, S.E., 2005: On the Question of the "Recovery" of the Rains in the West African Sahel. *J. Arid Envir.,* **63**, 615-641.

Nicholson, S.E., 2007a: On the factors modulating the intensity of the tropical rainbelt over West Africa. In preparation for *J. Climate*. (to be submitted 6/07)

Nicholson, S. E., 2007b: The intensity, location and structure of the tropical rainbelt over West Africa as a factor in interannual variability. In press, *Int. J. Climatology*.

Nicholson, S. E., and I. M. Palao, 1993: A re-evaluation of rainfall variability in the Sahel Part I. Characteristics of rainfall fluctuations. *Int. J. Climatology*, 13, 371-389.

Nicholson, S. E., and J. P. Grist, 2001: A simple conceptual model for understanding rainfall variability in the West African Sahel on interannual and interdecadal time scales. *Int. J. Climatology*, 21, 1733-1757.

Nicholson, S. E., and J. P. Grist, 2003: On the seasonal evolution of atmospheric circulation over West Africa and Equatorial Africa. *J. Climate*, 16, 1013-1030.

Nicholson, S. E., A. I. Barcilon, M. Challa, and J. Baum, 2007: Wave Activity on the Tropical Easterly Jet. In press, *J. Atmos. Sci*.

Norquist, D.C., E.E. Recker, and R. J. Reed, 1977: The energetics of African waves disturbances as observed during Phase III of GATE. *Mon. Wea. Rev.*, 105, 334-342.

Peng, S., and J. S. Whitaker, 1999: Mechanisms determining the atmospheric response to mid-latitude SST anomalies. *J. Climate*, 12, 1393-1408.

Redelsperger, J.-L. et al., 2002: Multi-scale description of a Sahelian weather system representative of the West African monsoon. *Quart. J. Roy. Meteor. Soc.*, 128, 1229-1257.

Reed, R. J., D. C. Norquist, and E. E. Recker, 1977: The structure and properties of African wave disturbances as observed during Phase III of GATE. *Mon. Wea. Rev.*, 105, 317-333.

Reed, R., A. Hollingsworth, W. Heckley, and F. Delsol, 1988: An evaluation of the performance of the ECMWF operational system in analyzing and forecasting easterly wave disturbances over Africa and the tropical Atlantic. *Mon. Wea. Rev.*, 116, 824-865.

Reeves, R., C. Ropelewski, and M. Hudlow, 1979: Relationships between large-scale motion and convective precipitation during GATE, *Mon. Wea. Rev.*, 107, 1154-1168.

Rennick, M. A., 1976: The generation of African waves, *J. Atmos. Sci.*, 33, 1955-1969.

Rennick, M.A., 1981: Some sensitivity experiments with and African wave model. *J. Atmos. Sci.*, 38, 106-113.

Ricciardulli, L., and P. D. Sardeshmukh, 2002: Local time- and space scales of organized tropical deep convection. *J. Climate*, 15, 2775-1790.

Simmons, A. J., 1977: A note on the instability of the African Easterly Jet, *J. Atmos. Sci.*, 34, 1670-1674.

Thompson, R.M., Jr., S. W. Payne, E. E. Recker, and R. J. Reed, 1979: Structure and properties of synoptic-scale wave disturbances in the intertropical convergence zone of the eastern Atlantic. *J. Atmos. Sci.*, 36, 53-72.

Tourre, Y.M., 1979: The squall line over West Africa and tropical eastern Atlantic ocean during GATE. PhD. dissertation, University of Virginia (Ref. No. 82-08502).

Thorncroft, C.D., and D. P. Rowell, 1998: Interannual variability of African wave activity in a general circulation model. *Int. J. Climatology*, 18, 1305-1323.

Thorncroft, C. D., and B. J. Hoskins, 1994: An idealized study of African easterly waves. Part I: A linear view. *Quart. J. Roy. Meteor. Soc.,* 120, 953-982.

Valdes, P., J., and B., J., Hoskins, 1989: Linear simulations of the time mean climatological flow, *J. Atmos. Sci.*, 46, 2509-2527.

Wang, B, 1988: Dynamics of tropical low-frequency waves: An analysis of the moist Kelvin wave. *J. Atmos. Sci.*, 45, 2051-2065.

Ward, M. N., 1998: Diagnosis and short-lead time prediction of summer rainfall in tropical North America at interannual and multidecadal timescales. *J. Climate*, 11, 3167-3191.

Xie, X., and B. Wang, 1996 Low-frequency equatorial waves in vertically sheared zonal flows. Part II: unstable waves. *J. Atmos. Sci.,* **53**, 3589-3605.

Xue, J., and J. Shukla, 1993: The influence of land surface properties on Sahel climate. Part I: Desertification. *J. Climate*, 6, 2232-2245.

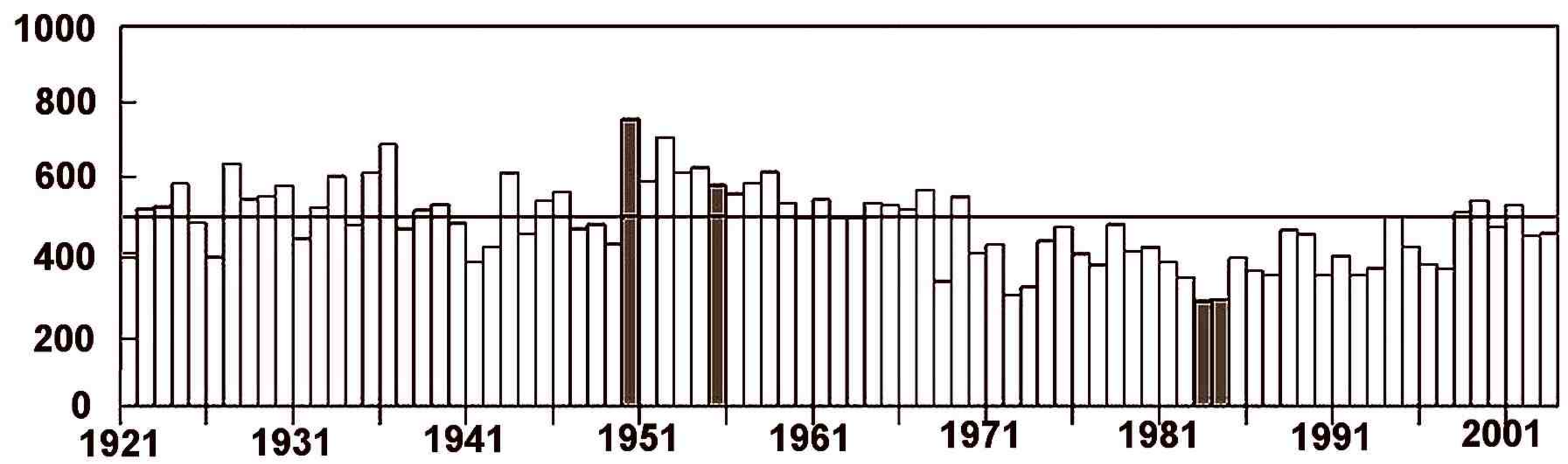

Figure 1. Rainfall in the Sahel 1901 to 2003, expressed as a regionally-averaged percent standard deviation (adapted from Nicholson 2005). The years used in this study are shaded: 1950, 1955, 1984 and 1983.

CONCEPTUAL MODEL

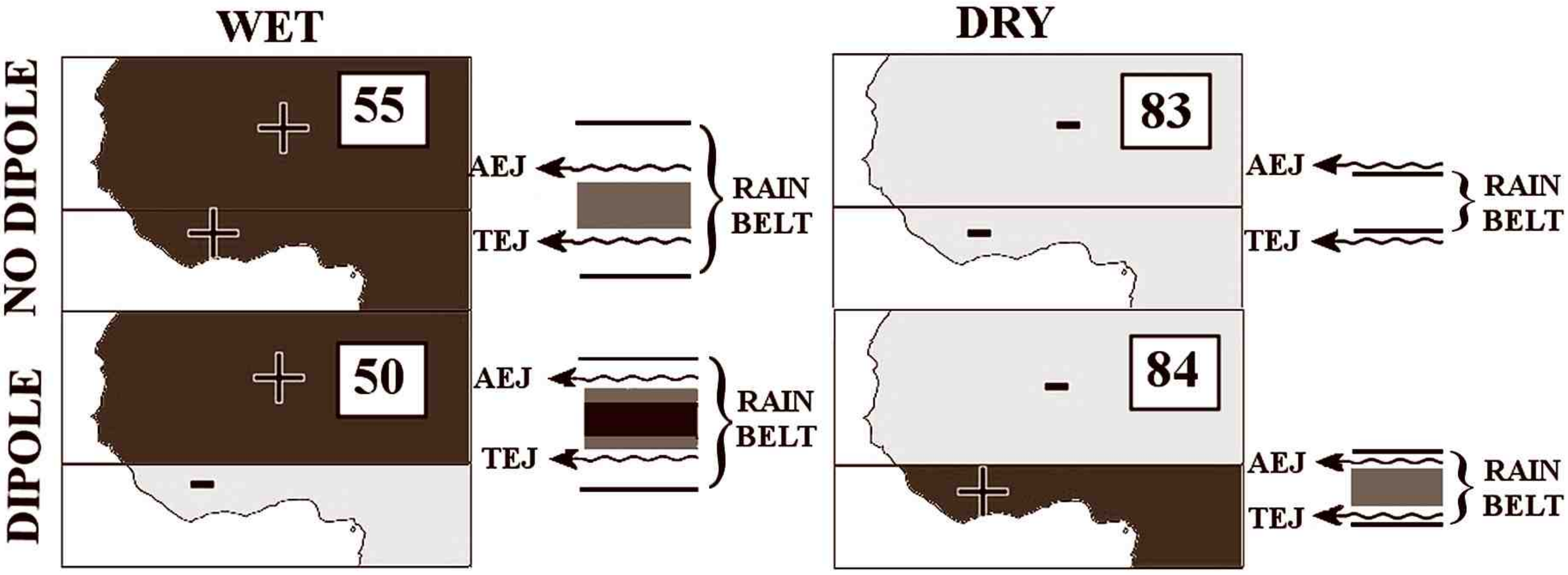

Figure 2. Conceptual model of rainfall variability sub-Saharan West Africa. Shading in the "rainbelt" indicates its core latitudes, with the degree of shading indicating intensity. Variations are a function of the intensity of the "rainbelt" and the latitudinal location of the AEJ, which determines the latitude of the rainbelt in the boreal summer. Changes in the intensity produce wet or dry conditions throughout, while shifts in the latitude of the AEJ produce the well-known rainfall dipole, with contrasting anomalies in the Sahel and Guinea Coast. Large numbers on the maps indicate the analysis year corresponding to the pattern. Note also the reduced latitudinal extent of the rainbelt in the dry years.

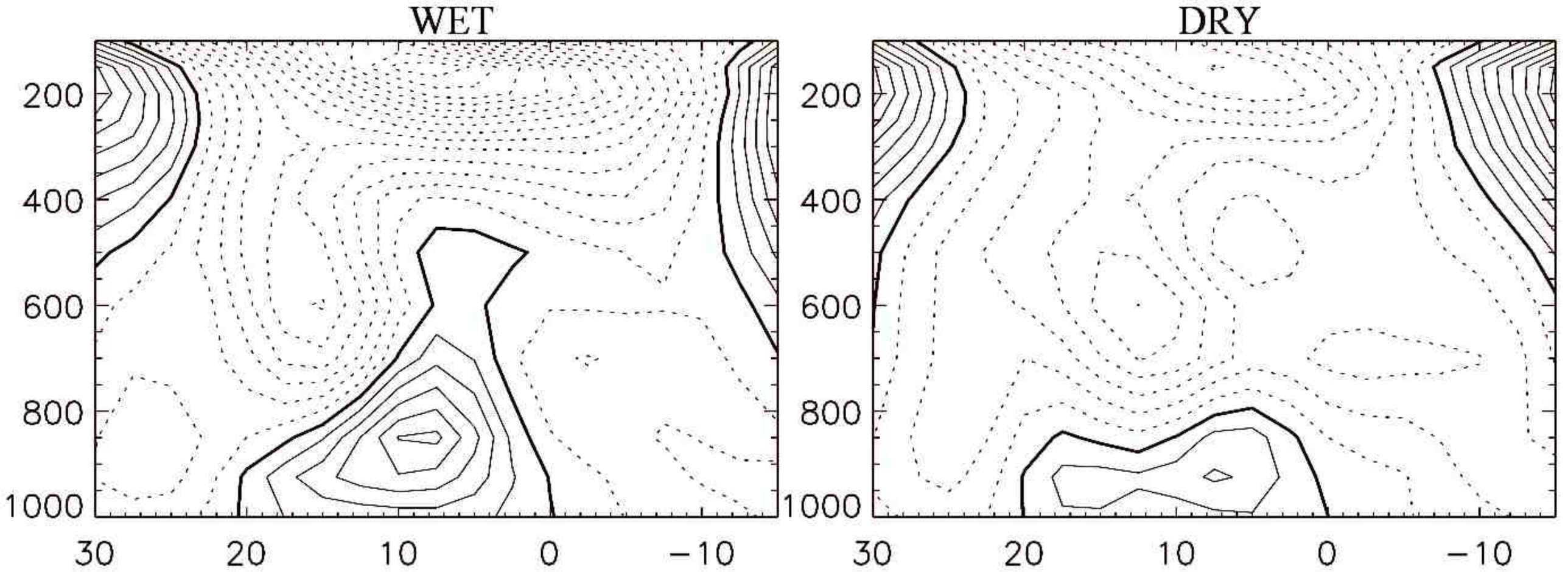

Figure 3. Mean zonal wind speed (m s^{-1}) averaged between 20 ^{o} E and 10 ^{o} W for August (from Grist and Nicholson 2001). A composite of four wet years (1958-1961) is compared with a composite of dry years (1982-1985). Contours correspond to 2 m s^{-1}.
Solid contours: westerlies; dashed contours: easterlies.

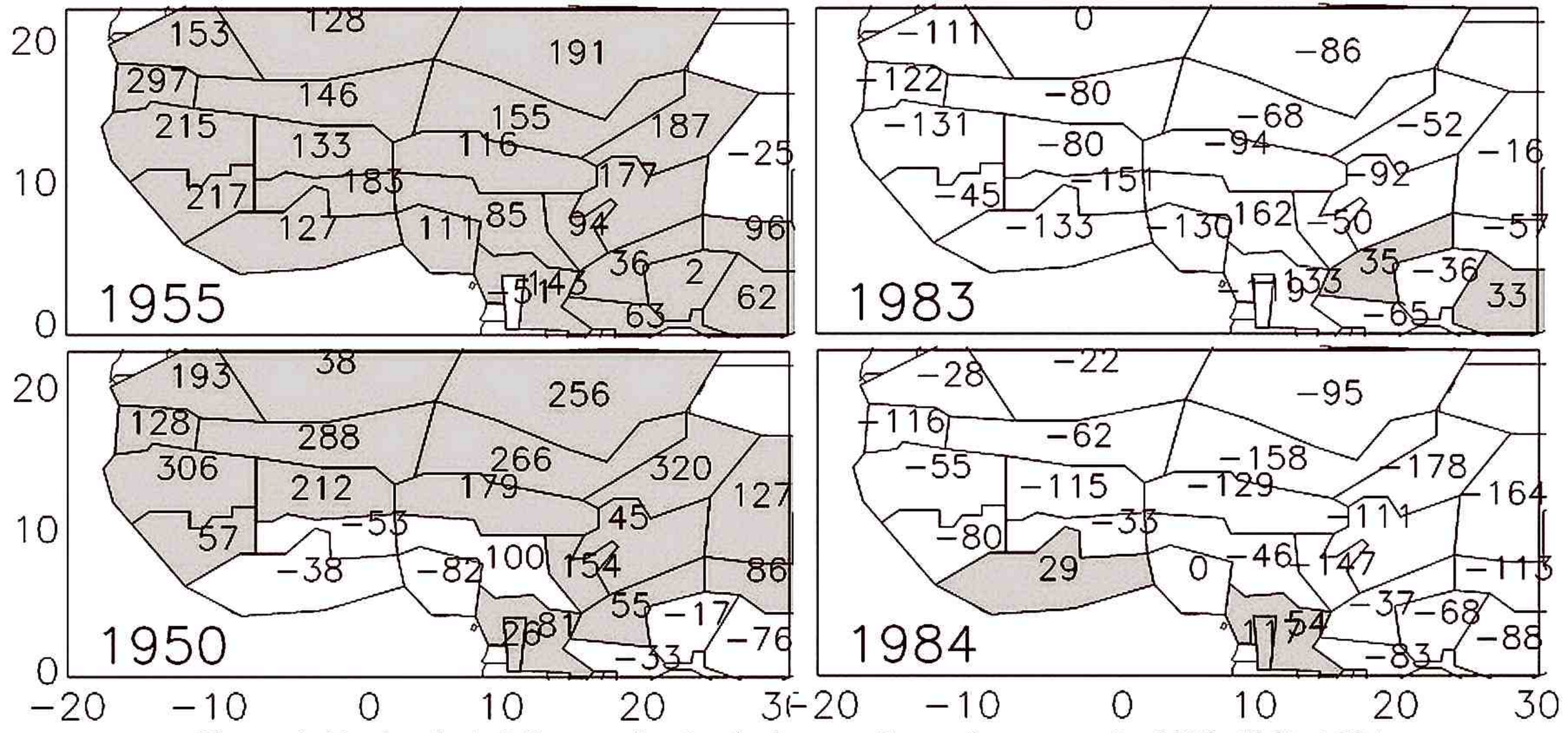

Figure 4. Regional rainfall anomalies for the June-to-September season for 1950, 1955, 1984 and 1983. Anomalies are expressed as a percent of the standard departure from the mean for the 30-years 1968-1997 (as in Nicholson 2007b).

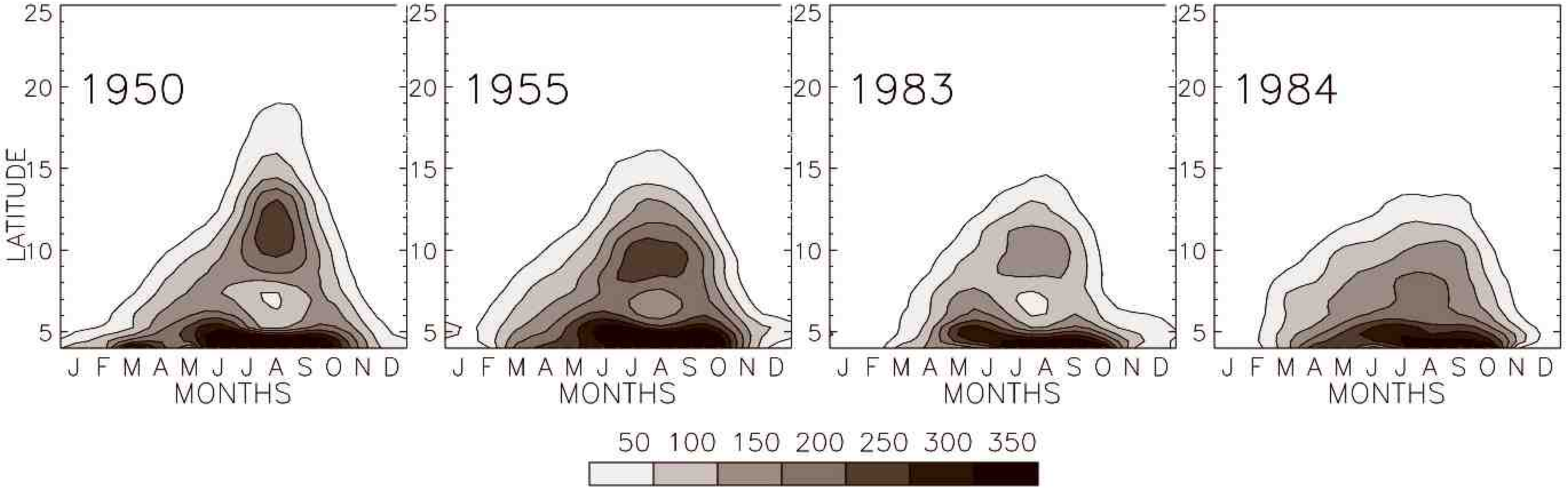

Figure 5. Rainfall as a function of month and latitude at 0 ^{o} W.

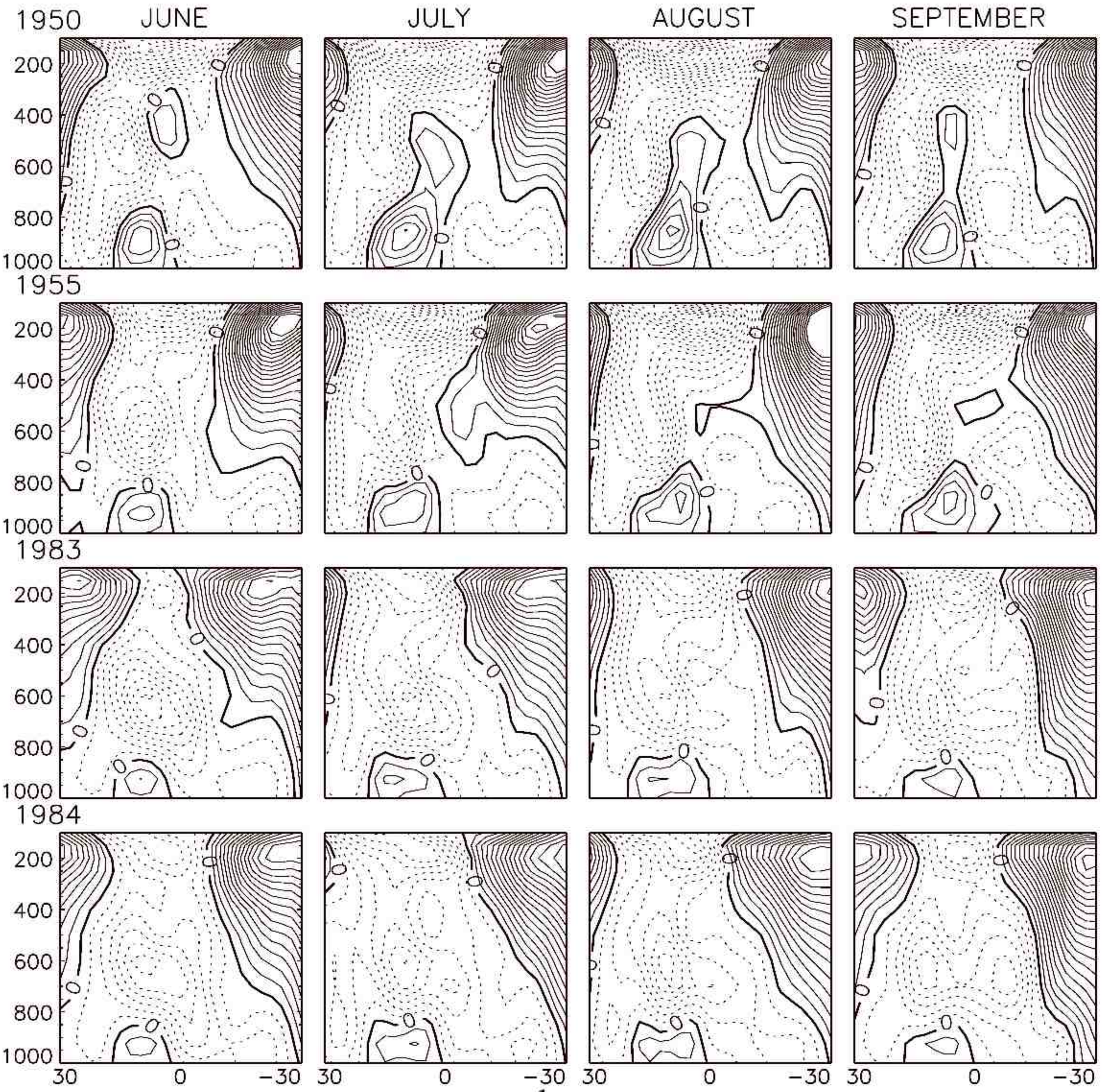

Figure 6. Mean zonal wind (m s^{-1}) of the basic state versus latitude for June through September of 1950, 1955, 1984 and 1983. Data are averaged between 10 ^{o} W and 10 ^{o} E; otherwise, as in Fig. 3.

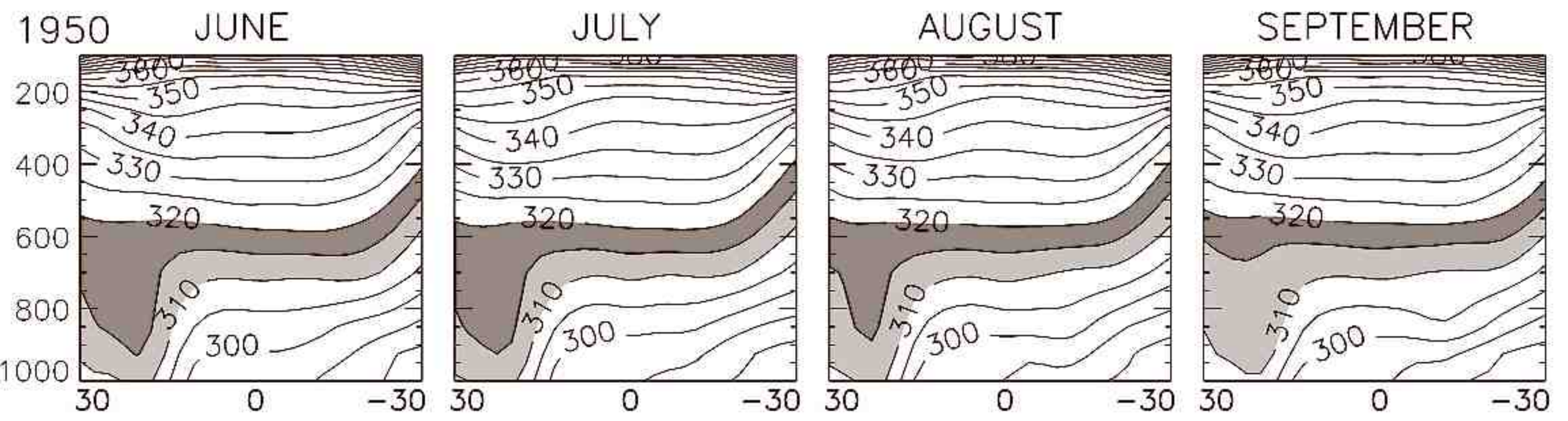

Figure 9. Plots of zonally-averaged potential temperature profiles between 31 ±latitudes as a function of pressure from 875 mb to 125mb for June through September of 1950. The data were selected in the band of longitudes between $\pm 10^{o}$ and extended around the globe. See text.

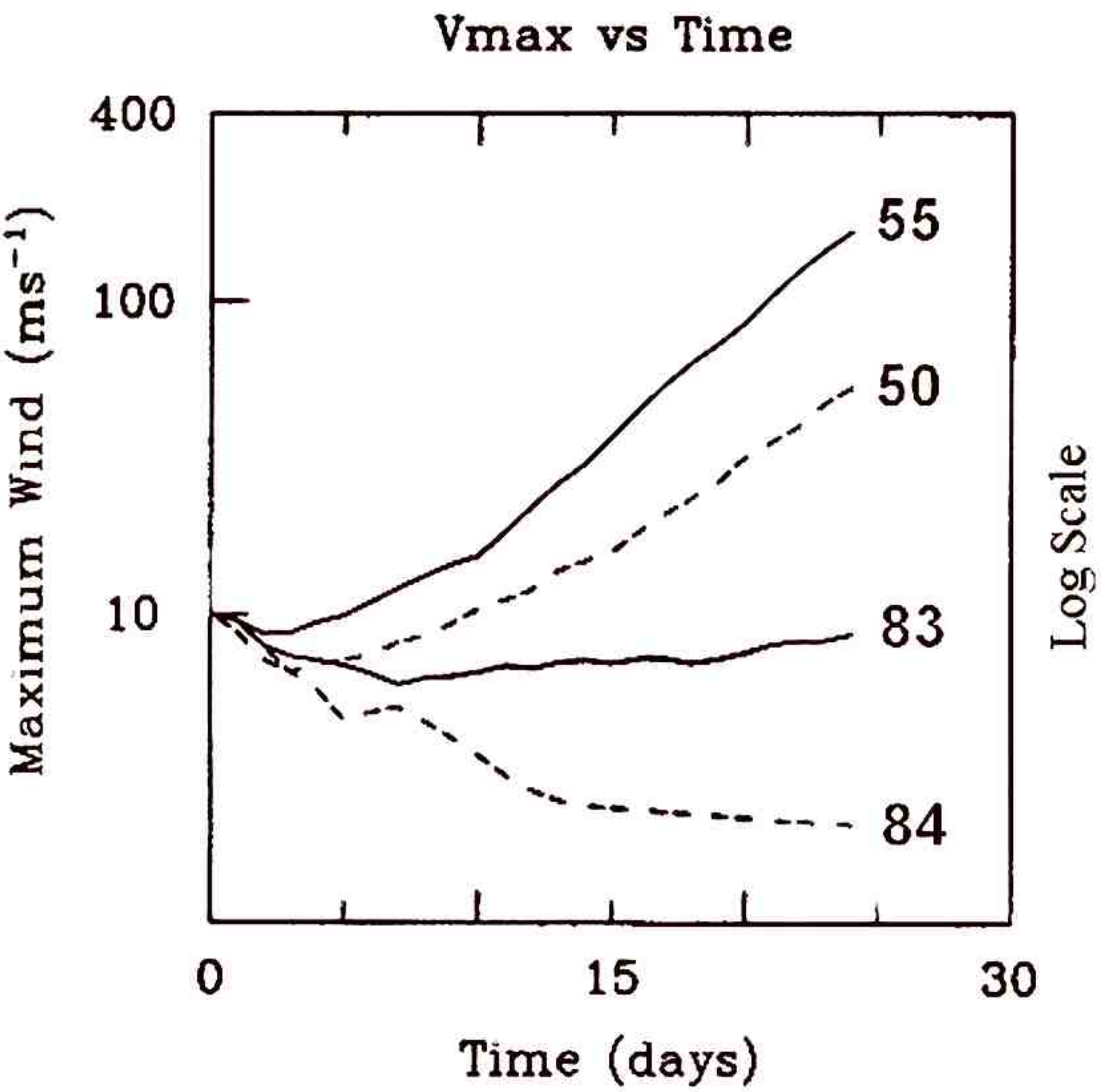

Figure 8. Wave growth vs. model day for August of the years 1950, 1955, 1984 and 1983.

Wave Growth Rate

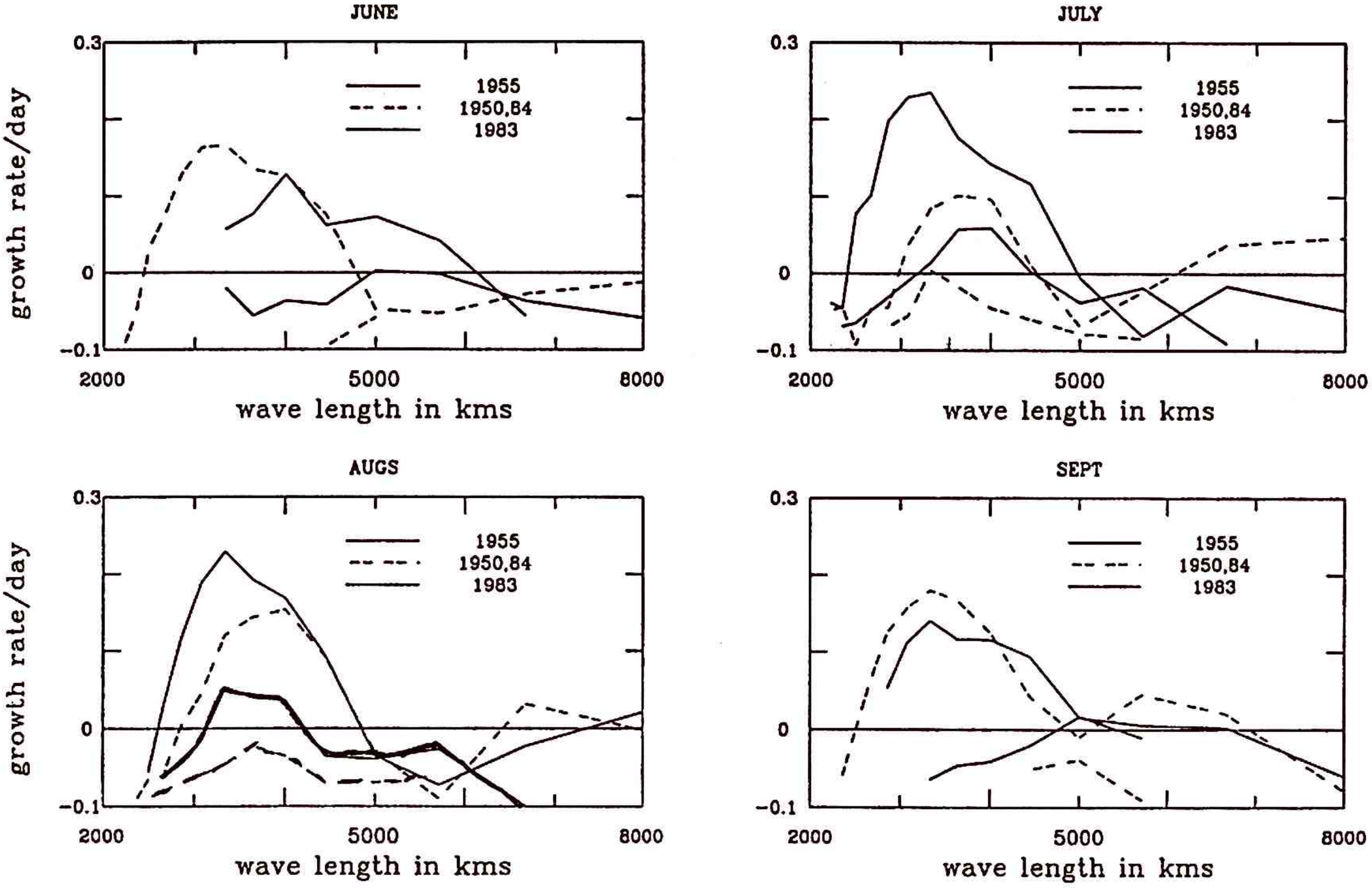

Figure 9 . Growth rates as a function of wavelength (in km) in June through September for the two wet years and two dry years. Wave growth rate vs. wave number on day 6; time shown is that corresponding to strongest wave activity during the day and varies with month and year.

JUNE

1955

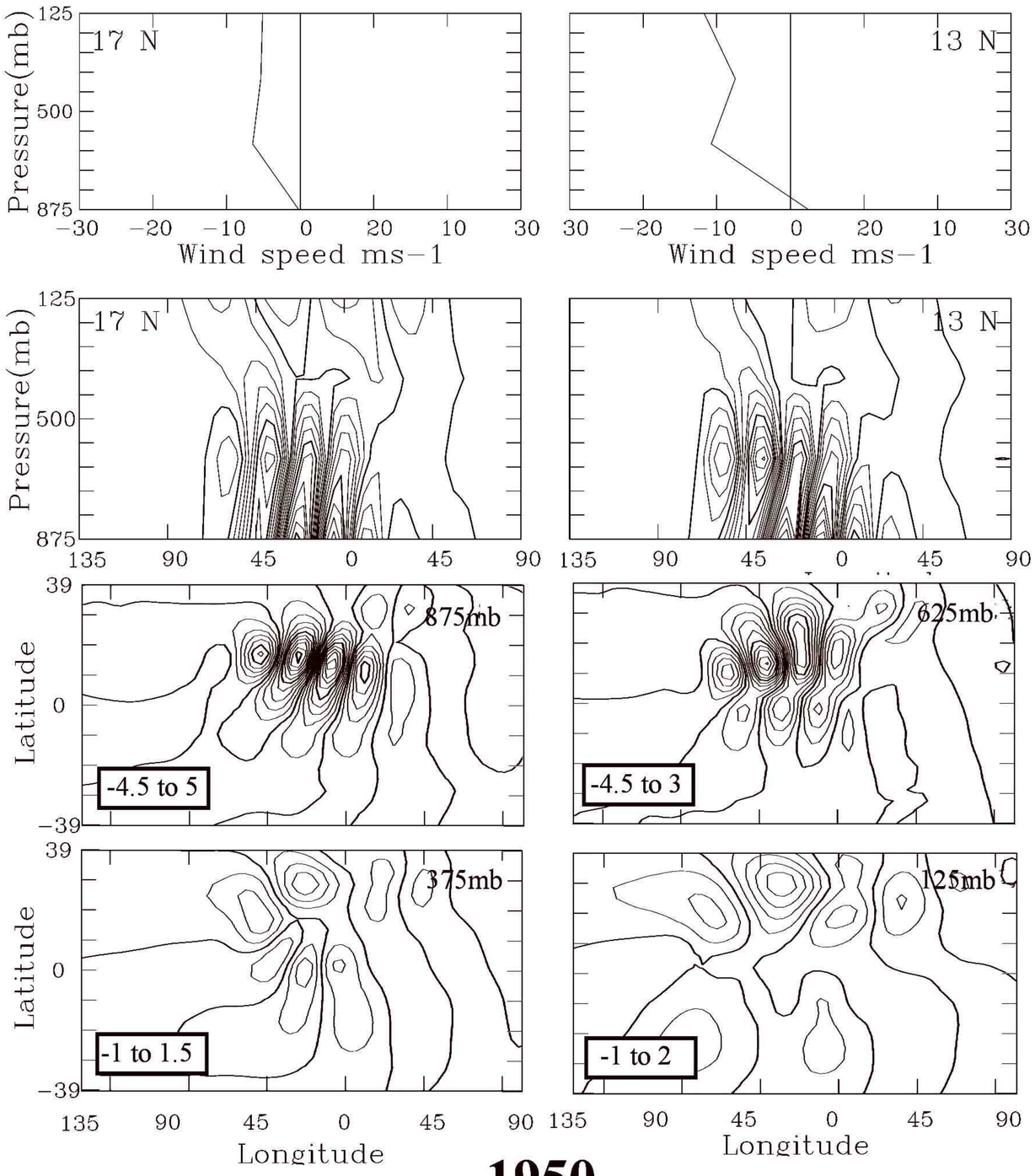

1983

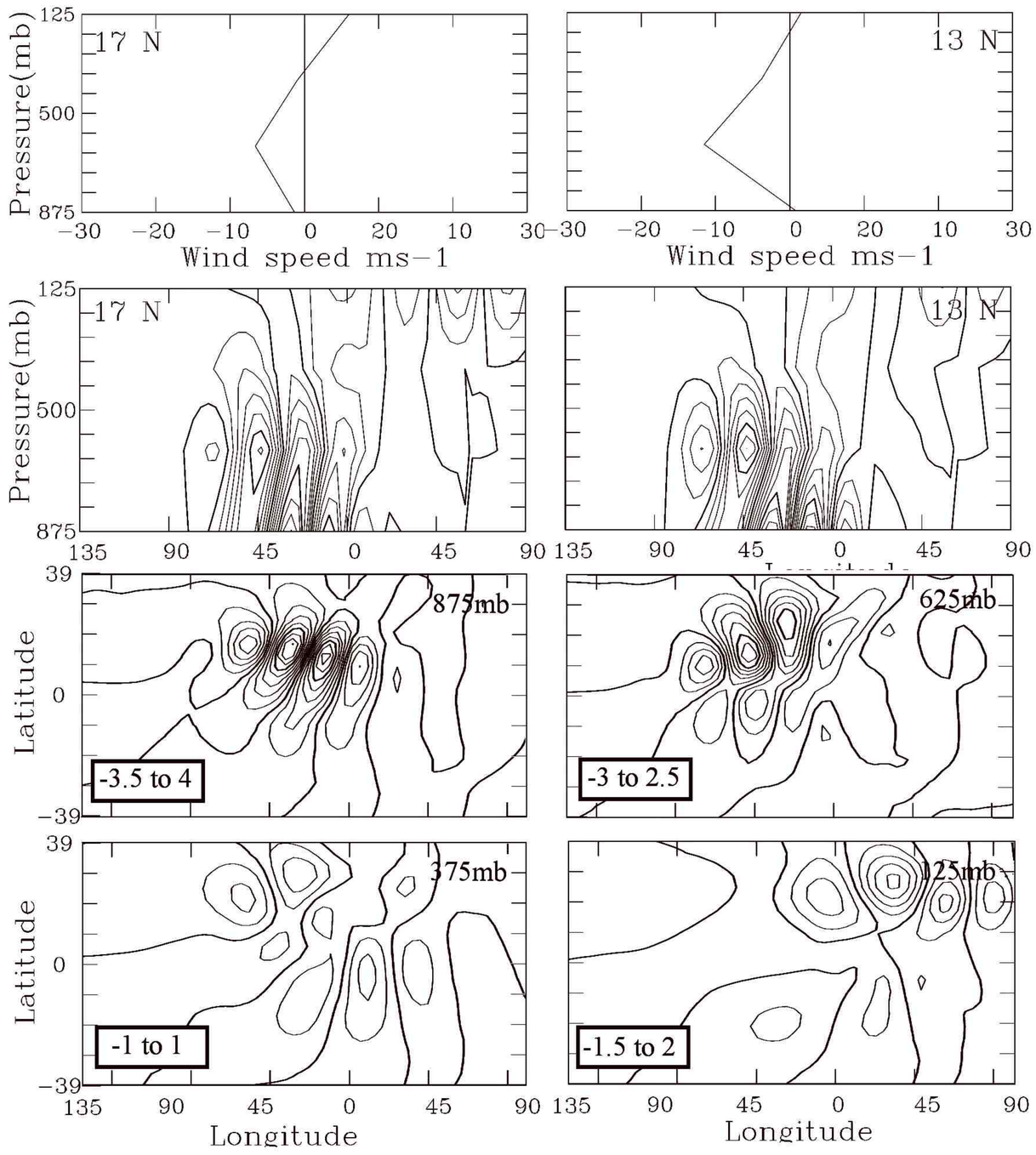

1950

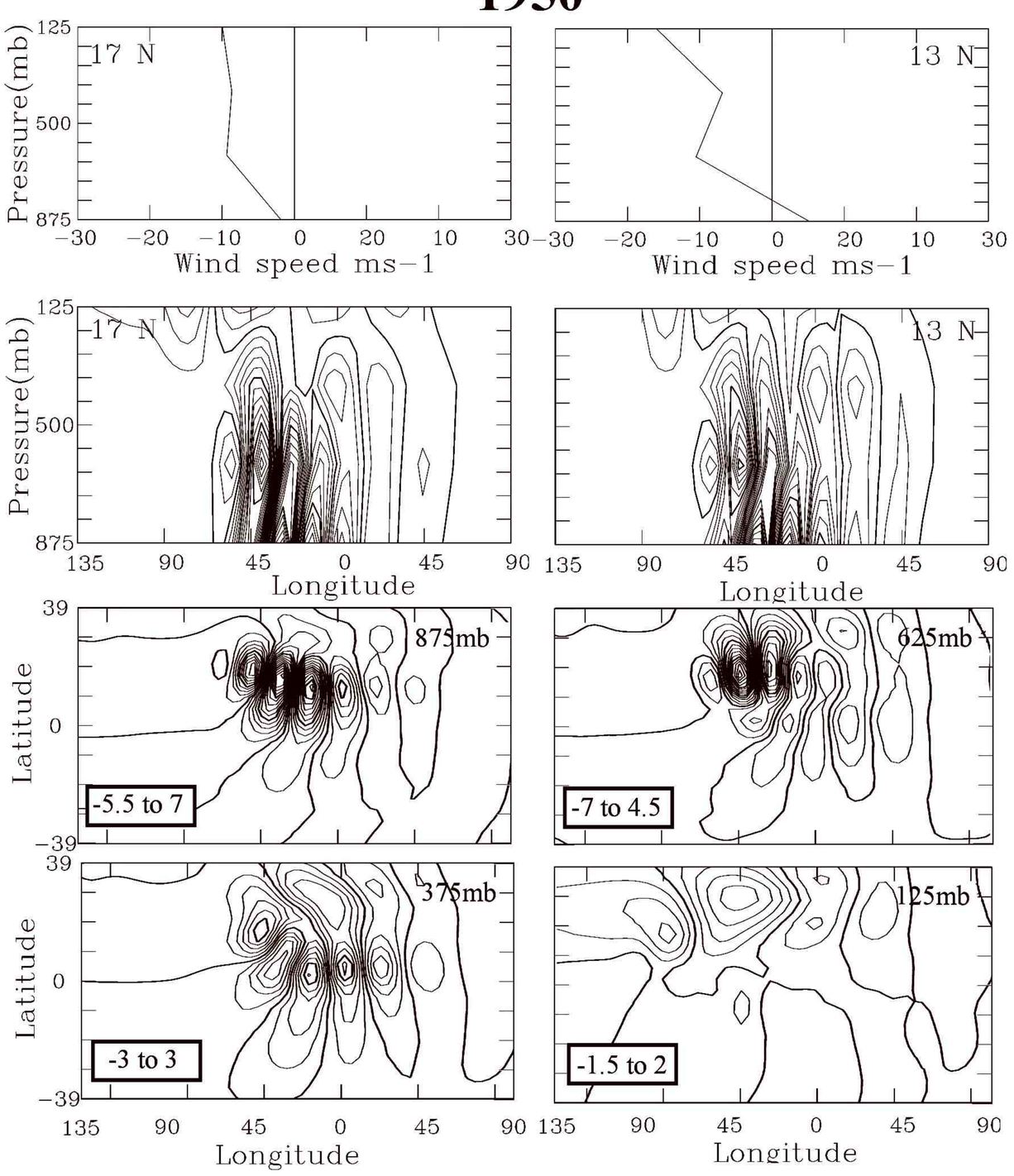

1984

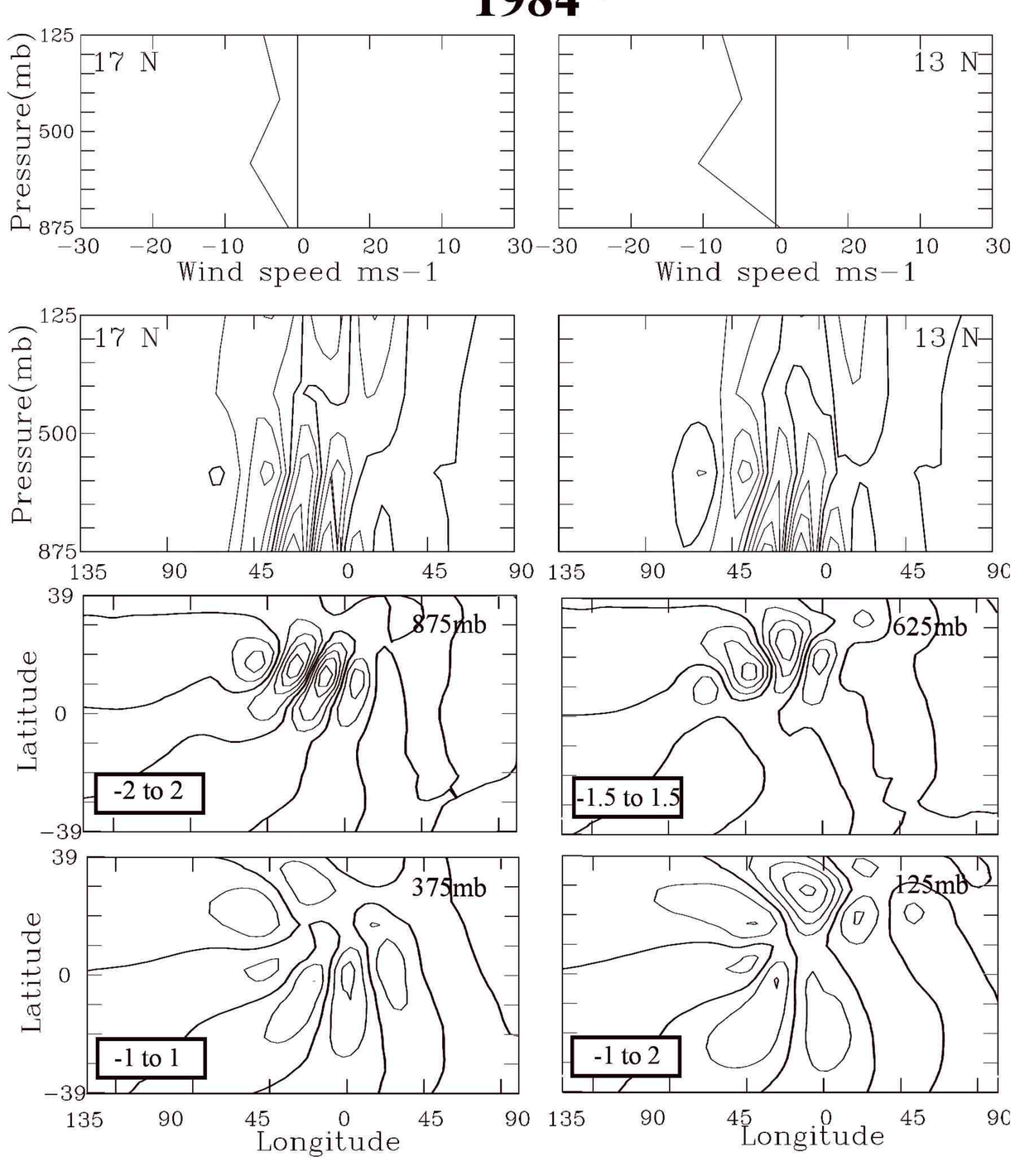

Figure 10. Results for June. Top: vertical profile of the zonal wind (m s-1) corresponding to the basic state. Center: Vertical profile of waves on day 6 as a function of longitude at the 17^{o} N and 13^{o} N. Bottom: wave activity as a function of latitude and longitude at four vertical levels (875 mb, 625 mb, 375 mb and 125 mb). Waves are expressed as the stream function (m^2s^{-1}), the magnitudes of which provide information on wave amplitude. The 0-contour is indcated in bold. To facilitate comparison of the four years, the maximum and minimum amplitudes of the stream function are indicated in boxes in the lower left of each frame. A longitude of 0^{o} corresponds to the longitude where the vortex was introduced and not the geographical longitude of 0^{o} . Note that only the longitudes from 135^{o} W to 135^{o} E are depicted; these longitudes are relative to the initial vortex.

JULY

1955

1983

1950

1984

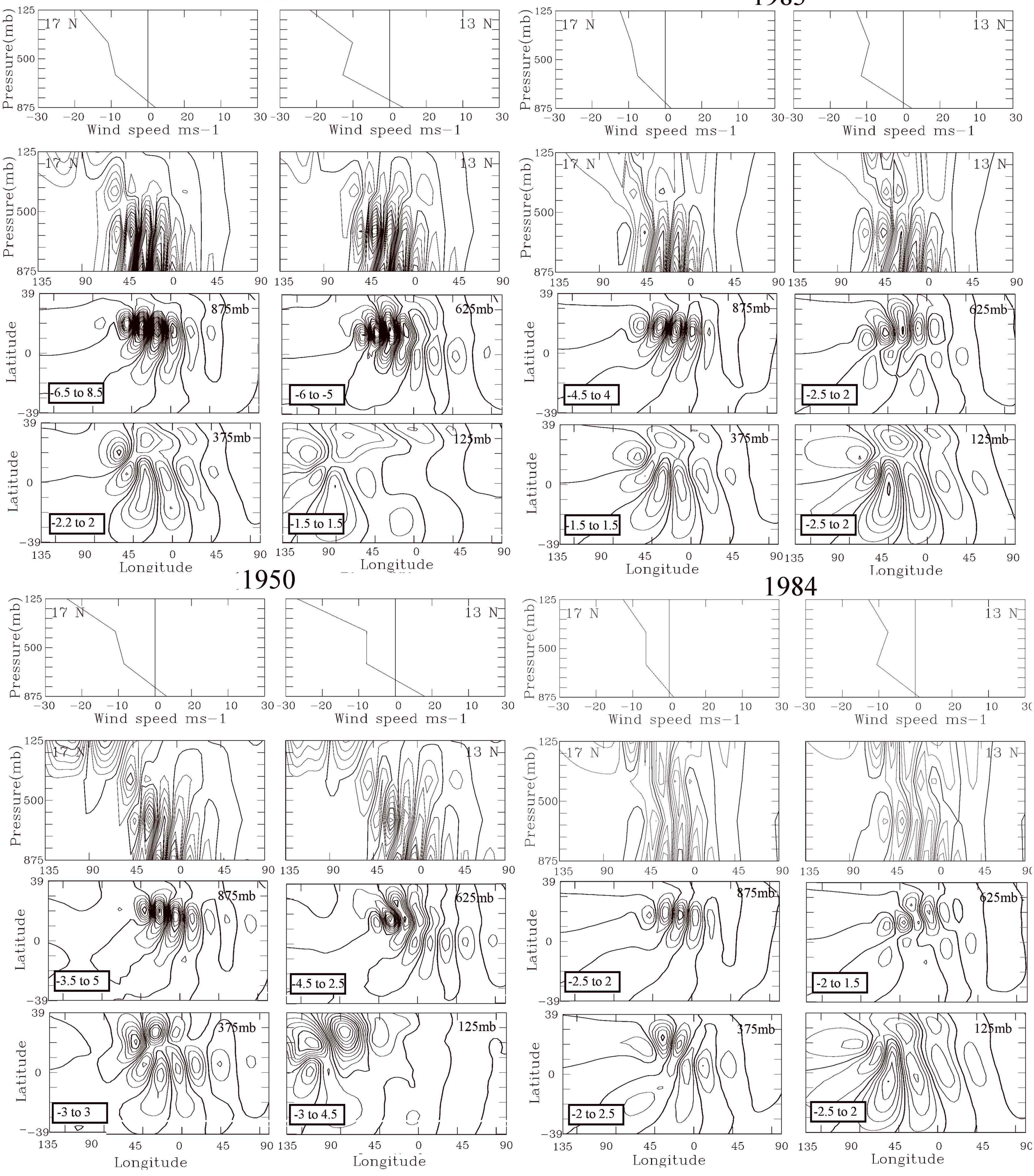

Figure 11. As in 10, but for July.

AUGUST

1955

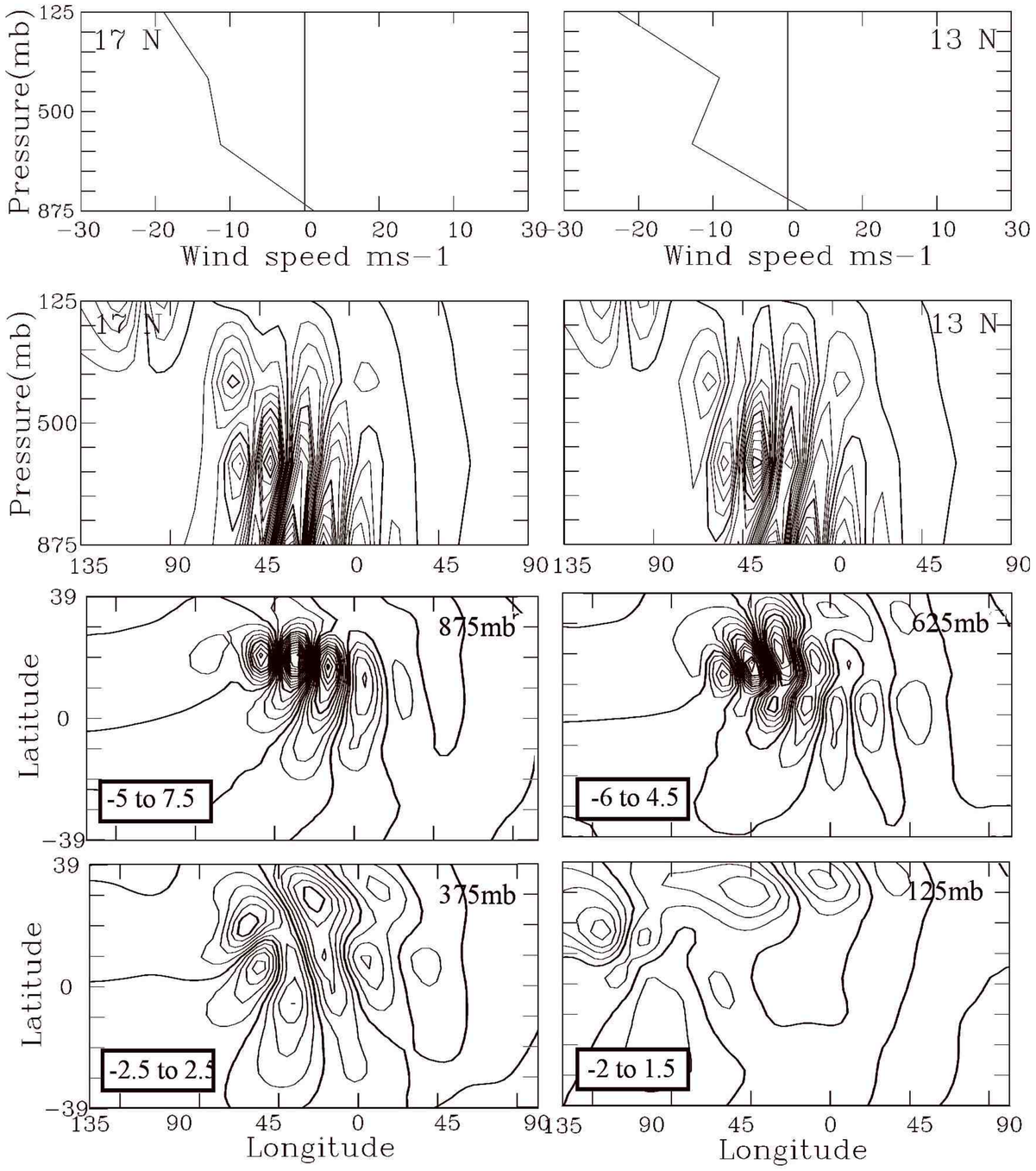

1983

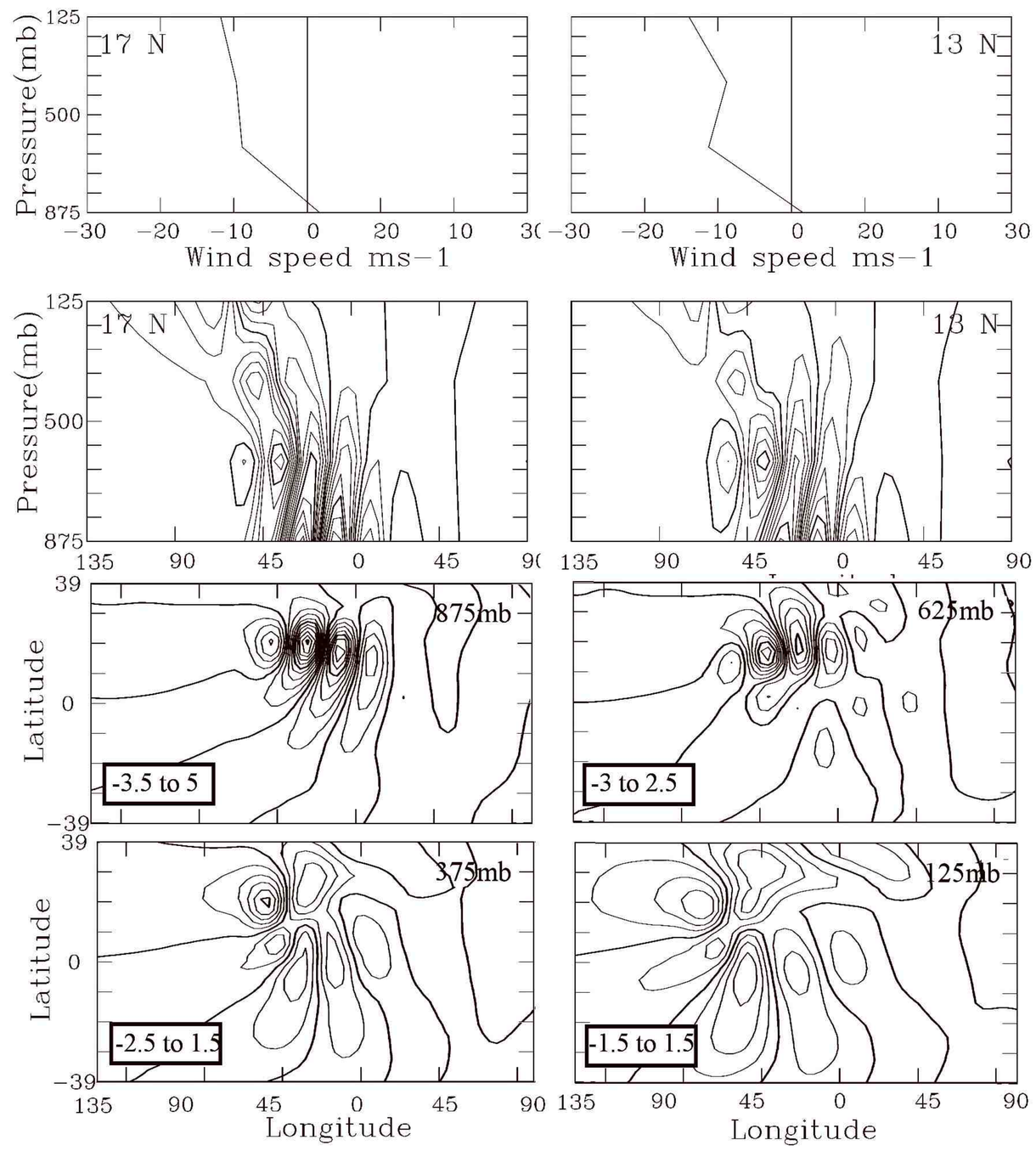

1950

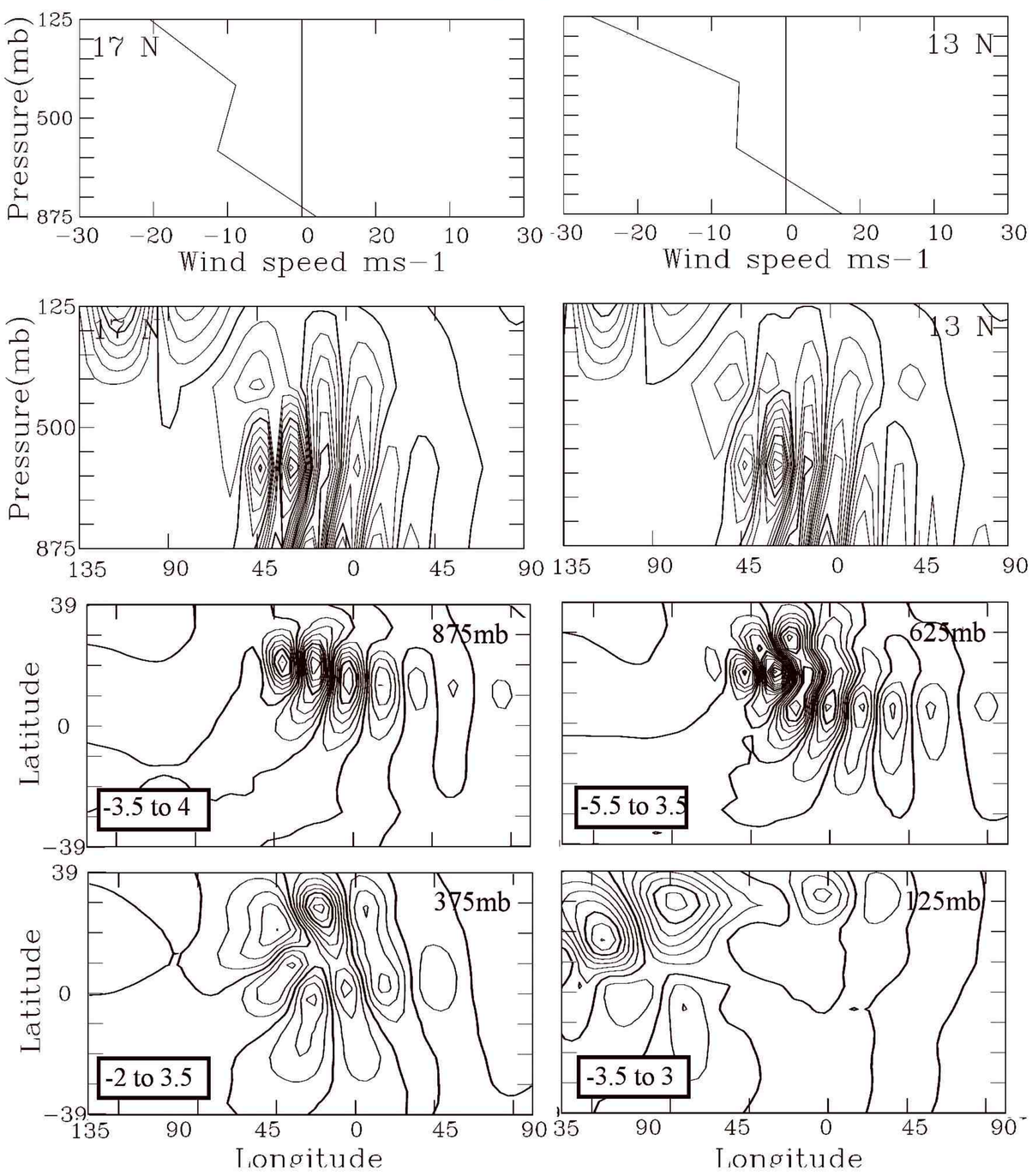

1984

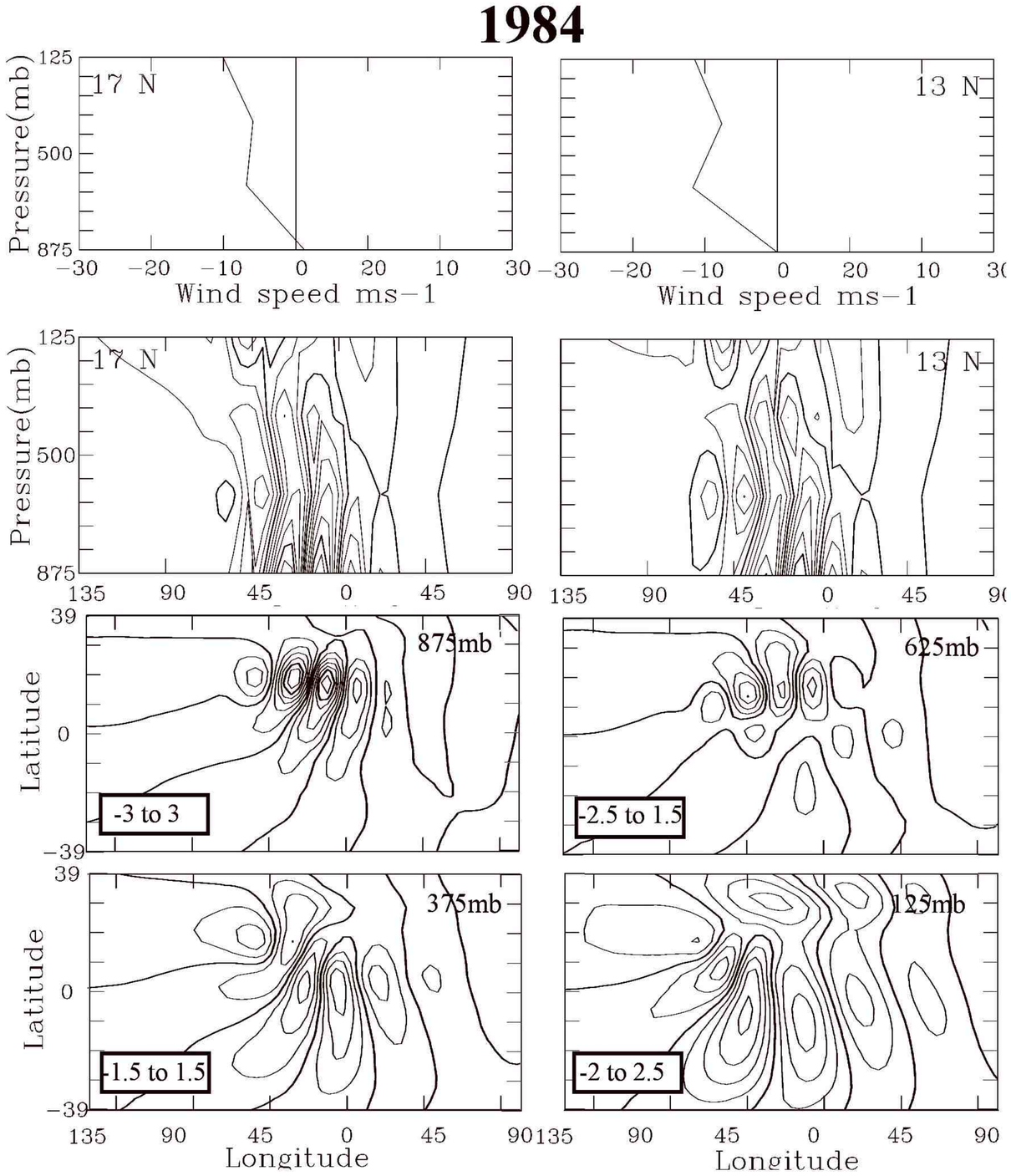

Figure 12. As in 10, but for August.

SEPTEMBER

1955

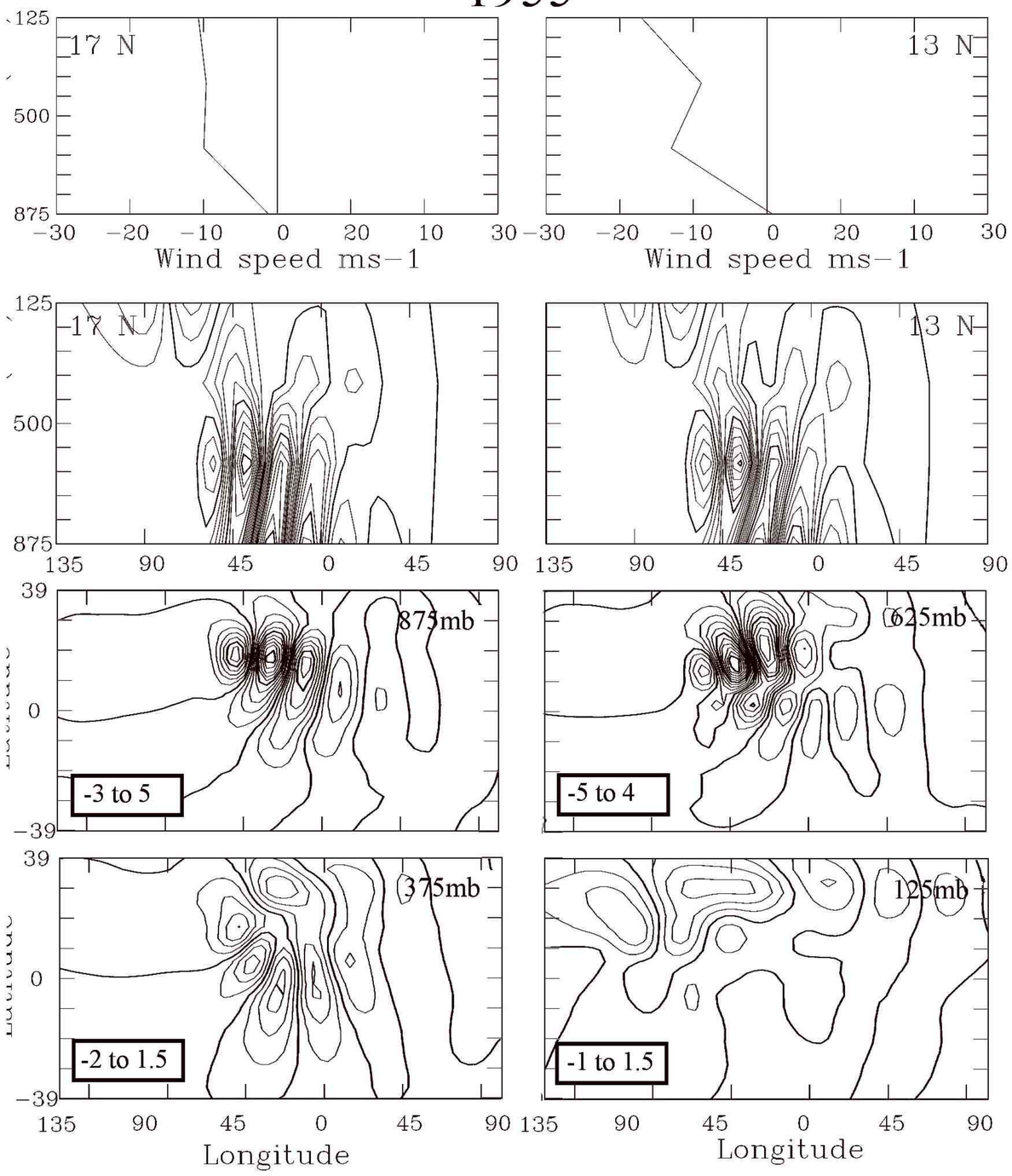

1983

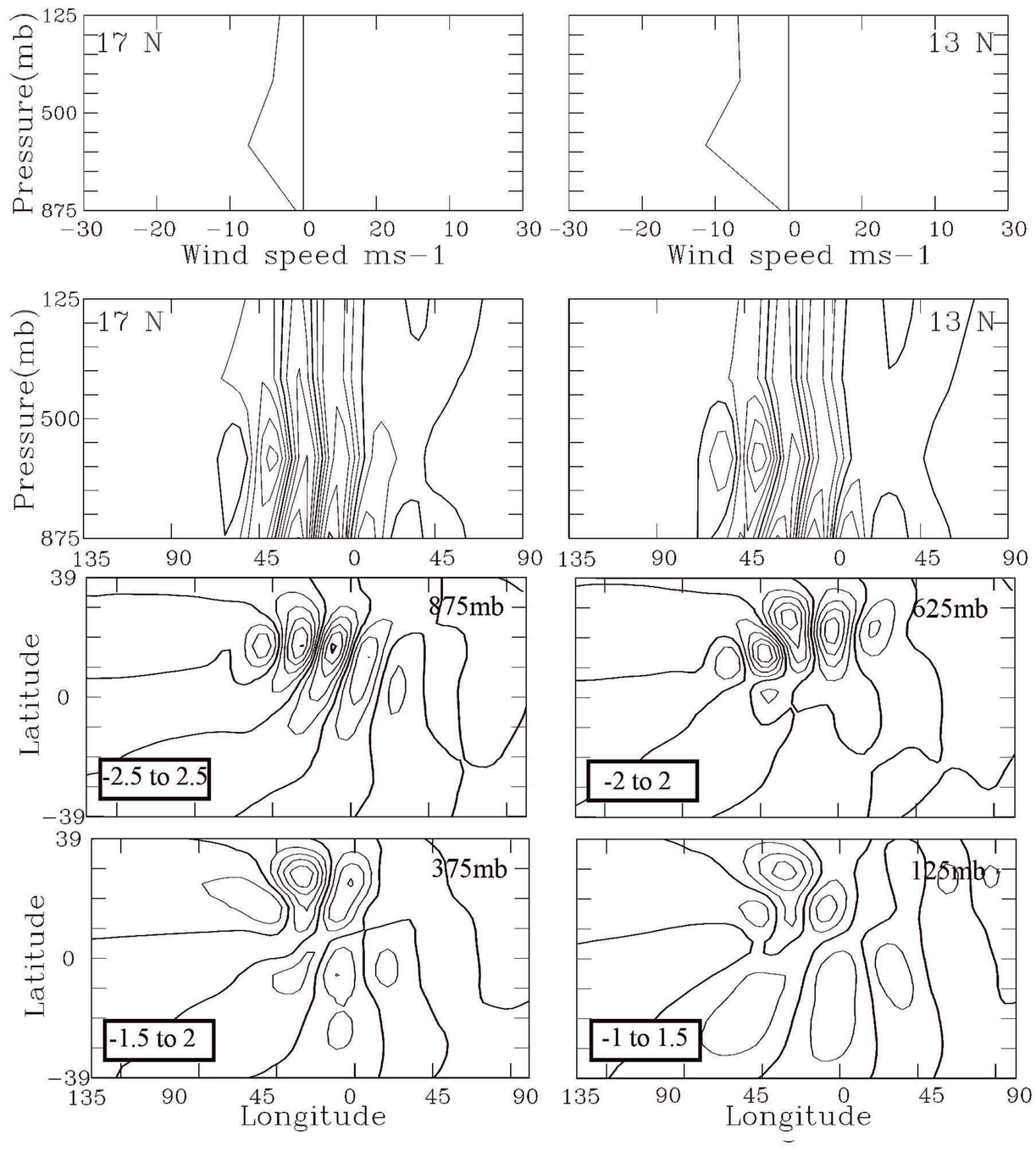

1950

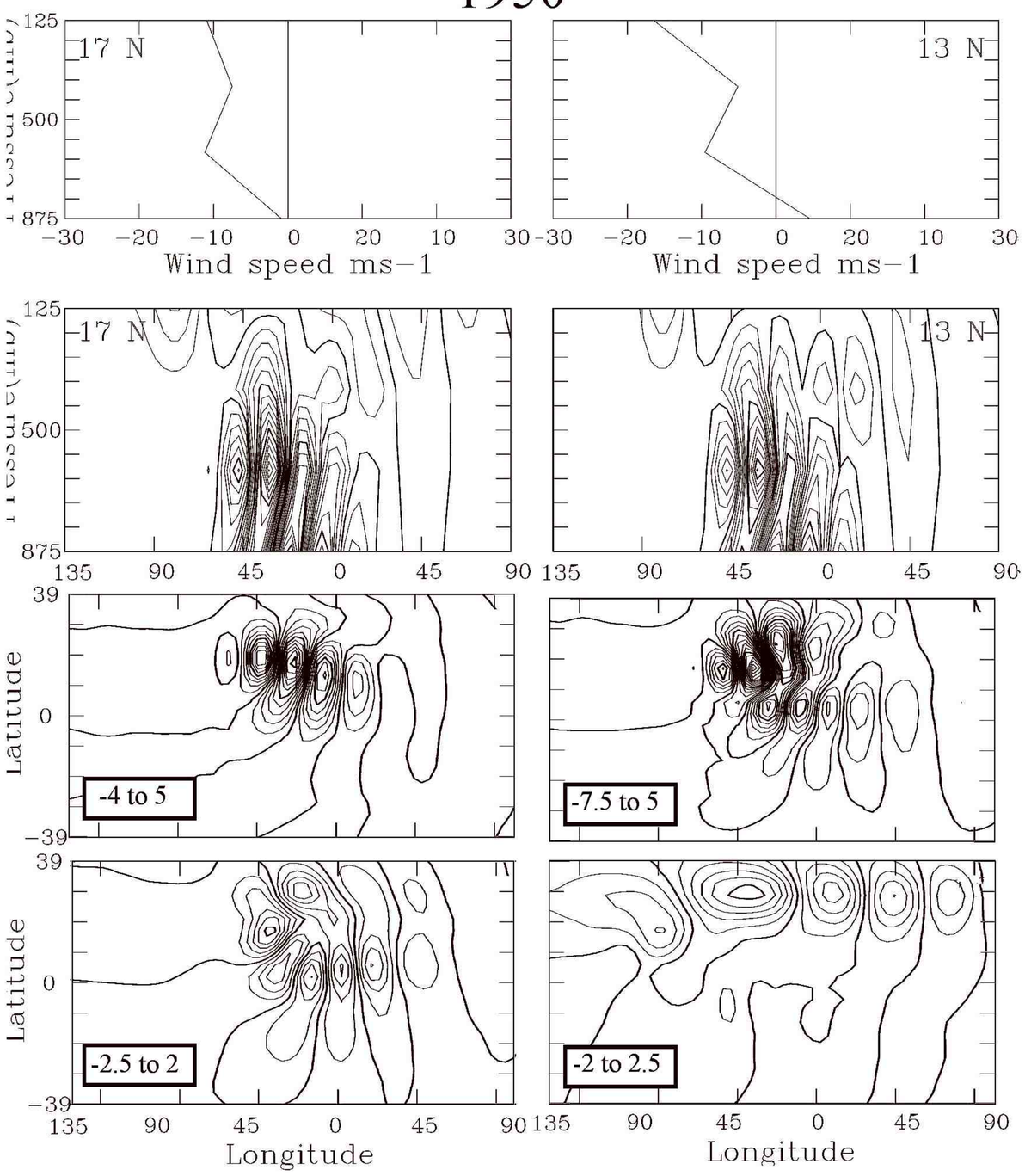

1984

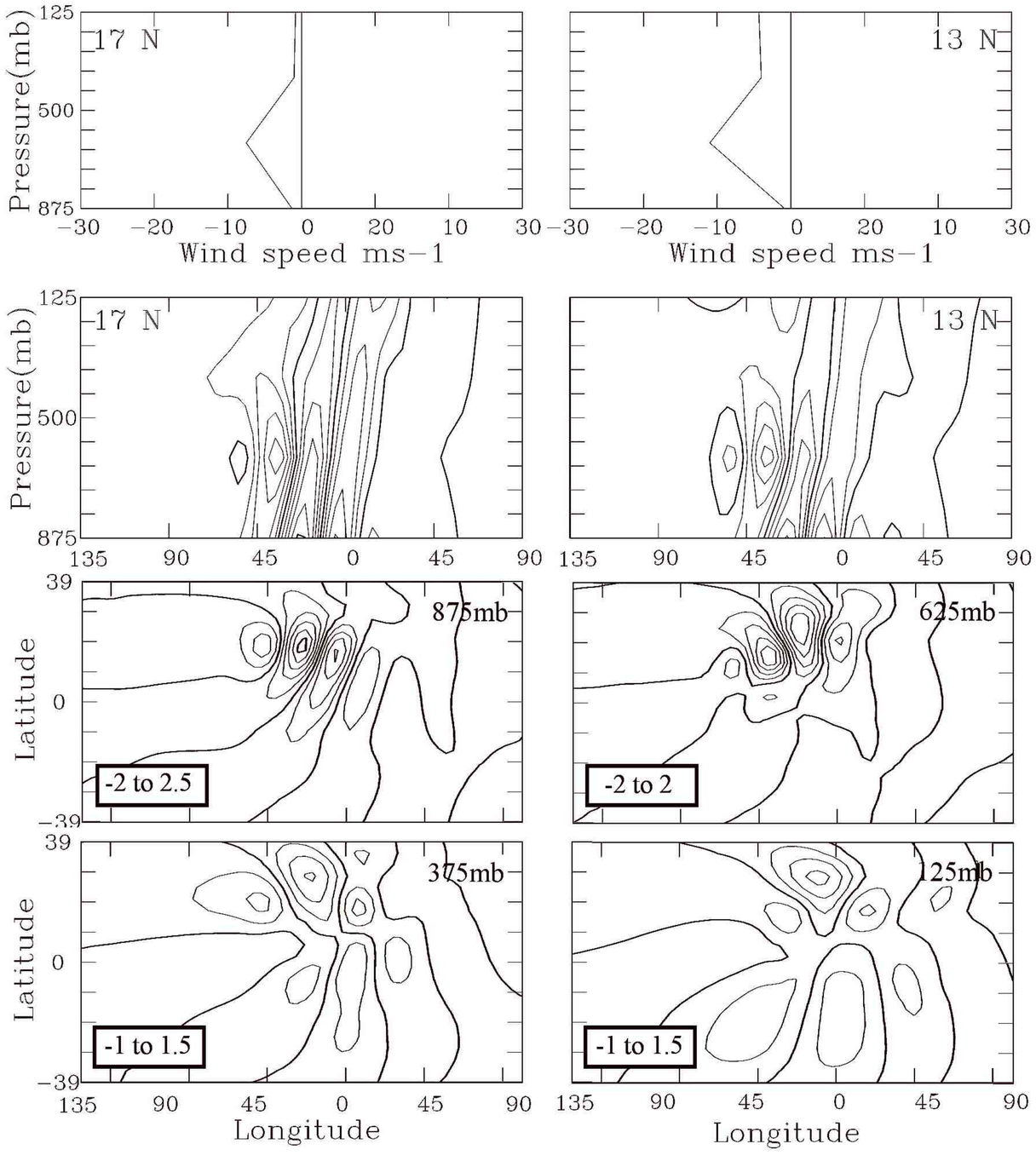

Figure 13. As in 10, but for September.

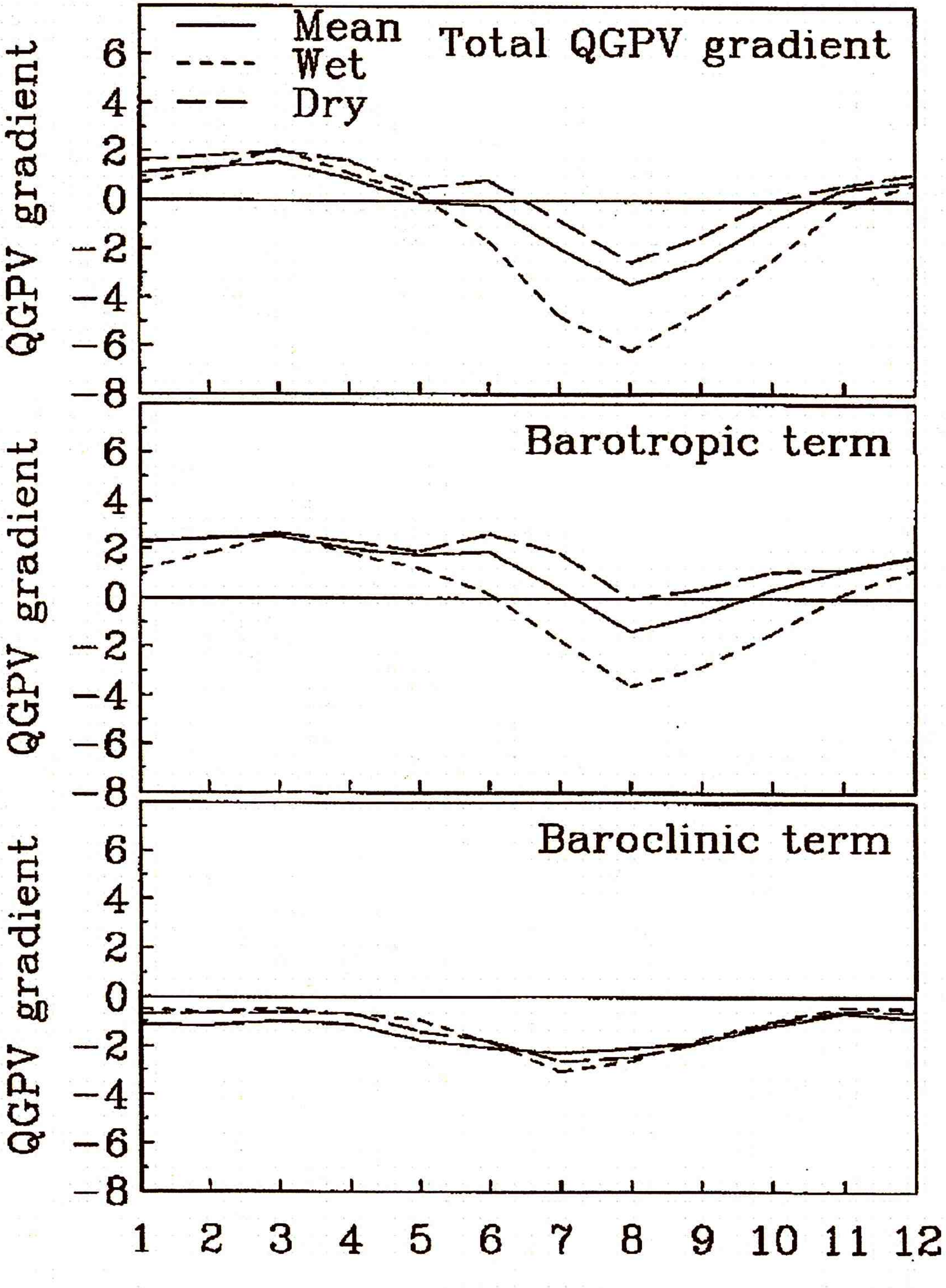

Figure 14. Quasi-geostrophic potential vorticity gradient (x 10-11 s-1), averaged between 10° W and 20° E at 15° N and 600 mb as a function of the month of the year. Solid line is 40-year mean, short dashed line is for wet years and long dashed line is for dry years. (a) Total QGPV gradient, (b) barotropic term, and (c) baroclinic term (from Grist 2002).

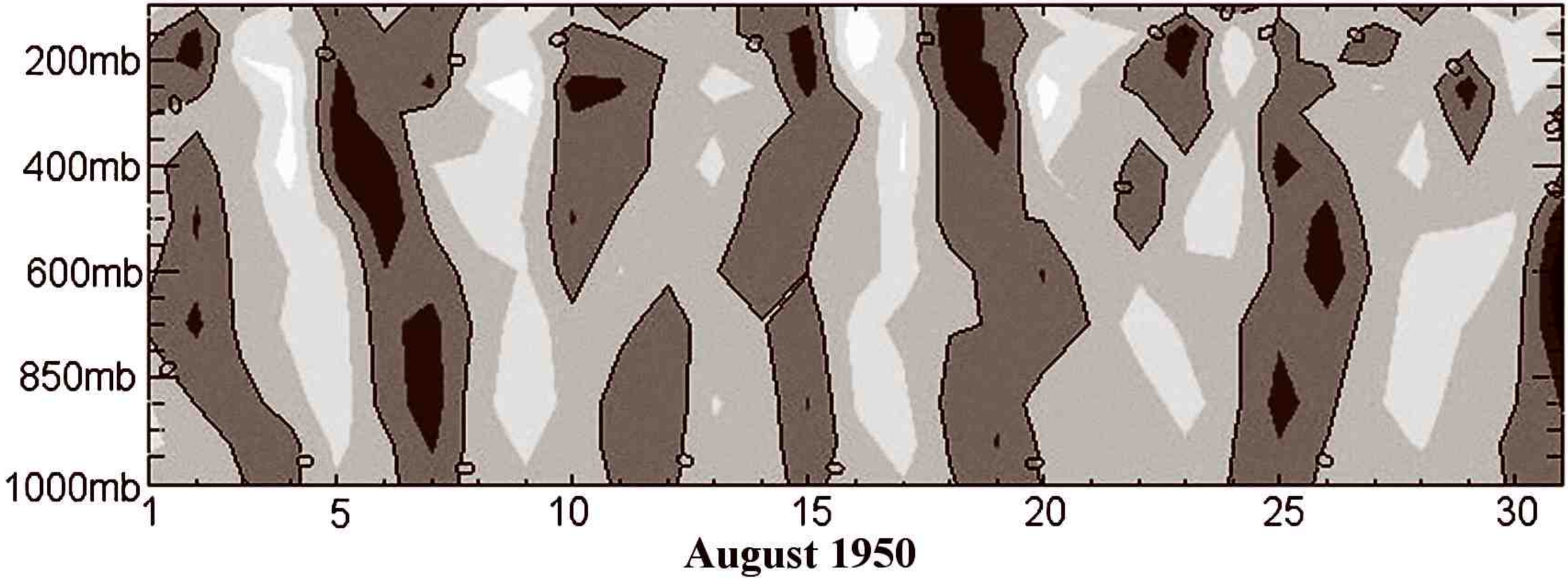

Figure 15. Hoevmueller diagram of filtered meridional wind at 10 ^{o} E for August 1950 (averaged for 12.5 ^{o} to 20 ^{o} N).

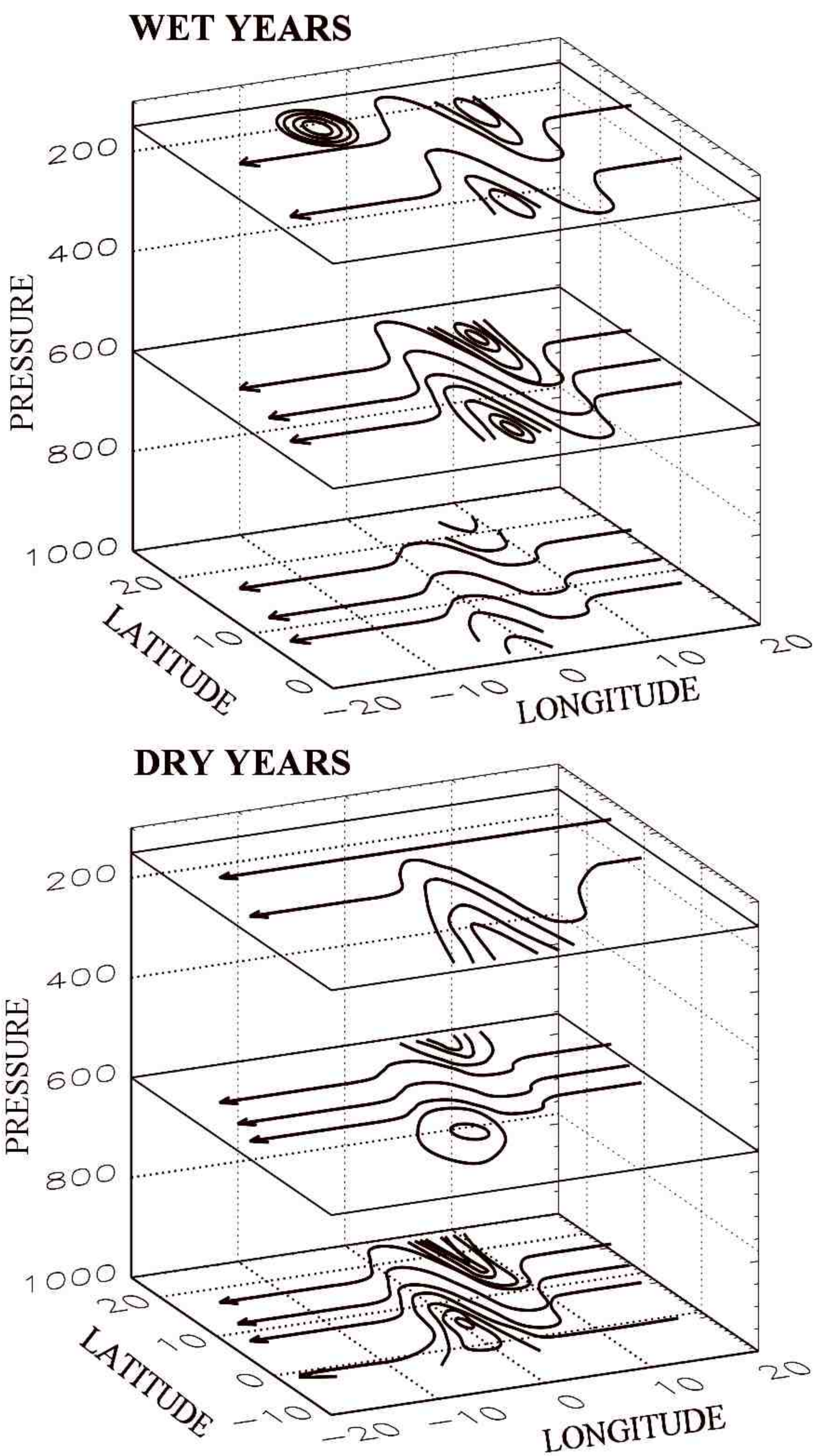

Figure 16. Schematic of wet year and dry year waves. Major contrasts are the level of maximum wave development, the degree to which the waves are developed at 150 mb, and the extension of waves at 150 mb into the southern hemisphere in dry years.